Exploiting Microstructural Instabilities in Solids and Structures: From Metamaterials to Structural Transitions

Dennis M. Kochmann
Department of Mechanical and Process Engineering,
ETH Zürich,
Leonhardstr. 21,
Zürich 8092, Switzerland;
Division of Engineering and Applied Science,
California Institute of Technology,
Pasadena, CA 91125
e-mail: dmk@ethz.ch

Katia Bertoldi
John A. Paulson School of Engineering and Applied Sciences,
Harvard University,
Cambridge, MA 02138;
Kavli Institute,
Harvard University,
Cambridge, MA 02138
e-mail: bertoldi@seas.harvard.edu

Instabilities in solids and structures are ubiquitous across all length and time scales, and engineering design principles have commonly aimed at preventing instability. However, over the past two decades, engineering mechanics has undergone a paradigm shift, away from avoiding instability and toward taking advantage thereof. At the core of all instabilities—both at the microstructural scale in materials and at the macroscopic, structural level—lies a nonconvex potential energy landscape which is responsible, e.g., for phase transitions and domain switching, localization, pattern formation, or structural buckling and snapping. Deliberately driving a system close to, into, and beyond the unstable regime has been exploited to create new materials systems with superior, interesting, or extreme physical properties. Here, we review the state-of-the-art in utilizing mechanical instabilities in solids and structures at the microstructural level in order to control macroscopic (meta)material performance. After a brief theoretical review, we discuss examples of utilizing material instabilities (from phase transitions and ferroelectric switching to extreme composites) as well as examples of exploiting structural instabilities in acoustic and mechanical metamaterials. [DOI: 10.1115/1.4037966]

1 Introduction

The long history of mechanics is rife with prominent examples of instabilities in solids and structures that have led to material failure or structural collapse, spanning all scales from atomic-scale void growth, failure, and stress-induced transformations to buckling and delamination in micro- and nano-electronics all the way up to tectonic events. Examples of causal mechanisms for mechanical instability are ubiquitous: buckling of structures, crushing of cellular solids, plastic necking, strain localization in shear or kink bands, wrinkling and crazing, void growth, fracture, and collapse. Through its more than 250-year-old history—going back to Euler's buckling studies [1–3] and involving such prominent mechanicians as Kirchhoff [4], Love [5], and the Lords Kelvin [6] and Rayleigh [7]—the theory of material and structural stability has resulted in analytical theories and numerical tools that have provided engineers with safe design guidelines. Starting with structures and advancing to continuous media within the frameworks of linear and later nonlinear elasticity as well as inelasticity, the theory of stability in solids and structures has evolved and resulted in many seminal contributions, see, e.g., Refs. [8–19] for a nonexhaustive list of classics in the field.

Over the past two decades, an exciting paradigm shift has been initiated away from traditional *design against instability* and toward novel *performance through controlled instability*: engineering mechanics is exploring the advantages of operating systems near, at, or beyond the critical point. (In)stability is instrumentalized for beneficial material or structural behavior such as, e.g., soft devices undergoing dramatic shape changes [20–22], propagating stable signals in lossy media [23] or controlling microfluidics [24], large reversible deformation of cellular solids [25,26], morphing surfaces and structures [27,28], high-damping devices and energy-absorbing technologies from nanotubes to macrodevices [29–32], acoustic wave guides and metamaterials [33–36], composites with extreme viscoelastic performance [37–40], or materials with actively controllable physical properties [41,42]. Especially at the macroscopic level, structural instability and the associated large deformation of soft matter have produced many multifunctional devices that exploit buckling, snapping, and creazing to result in beneficial acoustic or mechanical performance, see Ref. [43] for a recent survey. Like in structures, instability at the material level stems from non-(quasi)-convex energy landscapes [44,45]; here, however, instability is not tied to multiple stable or metastable structural deformation modes but involves multiple stable microstructural configurations such as those in phase transitions and phase transformations [46], domain switching and domain patterning [47–49], deformation twinning [50,51], or strain localization, shear banding, and patterning in plasticity [52]. From a mathematical standpoint, non-(quasi)convex energetic potentials entail instability of a homogeneous state of deformation, thus leading to energy-minimizing sequences which, physically, translate into complex microstructural patterns, see, e.g., Refs. [49] and [52–56].

In addition to structures and materials, metamaterials—somewhere in the diffuse interface between solids and structures—have gained popularity in recent decades. These engineered media commonly have a structural architecture at smaller scales, which is hidden at the larger scale where only an effective medium with effective properties is observed. The advent of additive manufacturing has fueled the design of complex metamaterials, see, e.g., Refs. [57–59], with instabilities now occurring across multiple scales.

Here, we present a survey of exploiting instabilities in solids and structures. Since the field has grown tremendously in recent years, we limit our review to concepts that exploit microscale instabilities to effect macroscale behavior, which applies to both structures (e.g., trusses or architected metamaterials) and materials (e.g., composites and other heterogeneous solids). The effective, macroscopic properties of heterogeneous solids and metamaterials are commonly identified by averaging over a representative volume element (RVE), including asymptotic expansions [60,61], numerical tools based on periodic boundary conditions (BCs) [62–65], as well as various upper and lower bounds on effective properties, especially for linear properties such as the (visco)elastic moduli, see, e.g., Ref. [66]. Besides the quasi-static mechanical

Manuscript received May 4, 2017; final manuscript received September 13, 2017; published online October 17, 2017. Editor: Harry Dankowicz.

properties such as stiffness, strength, and energy absorption, a major focus of architected metamaterials has been on wave motion. Here, the effective wave propagation characteristics of periodic, microstructured media can be obtained from the dispersion relations computed at the RVE level [67,68]. Unlike in conventional continuous media, structural metamaterials such as multiscale truss lattices can be exploited to independently control elastic moduli and dispersion relations [69]. We note that if the wavelength approaches the RVE size (in particular in acoustic metamaterials), classical homogenization approaches may lose their validity, which is why new theories have been proposed for the effective property extraction in more general settings, e.g., see Refs. [70–75], which is closed under homogenization and can be linked to Bloch–Floquet analysis [76]. Alternatively, computational techniques have obtained the effective dynamic performance even in transient, nonlinear, or inelastic settings [77,78]. These concepts have been applied to both materials and structures, resulting in interesting, extreme, peculiar, or controllable effective (meta)material properties to be reviewed in the following.

We first give a concise review of the fundamental concepts of stability theory to the extent required for subsequent discussions, followed by a survey of first material and then metamaterial strategies that take advantage of instability. Finally, we discuss the state-of-the-art and point out ongoing directions and topical opportunities.

2 Stability Theory

2.1 Notions of Stability. From a theoretical viewpoint, stability problems have traditionally been treated by either *energetic principles*, linking stability to the uniqueness of solutions or minima in the potential energy landscape [79–81] or alternatively by *dynamic analysis*, defining stability as bounded solutions over time in the sense of Lyapunov [82,83]. Both definitions coincide for conservative systems under small perturbations [84] but may deviate otherwise (e.g., in the presence of gyroscopic forces [85]) where only dynamic methods generally yield the correct stability conditions [86].

For a dynamical system characterized by $\partial \mathbf{u}/\partial t = \mathbf{f}(\mathbf{u}, t, \gamma)$ with unknown variables $\mathbf{u} \in \mathbb{R}^n$, time $t \in \mathbb{R}$, control parameter $\gamma \in \mathbb{R}$, and generally nonlinear driving forces $\mathbf{f}: \mathbb{R}^n \times \mathbb{R} \times \mathbb{R} \to \mathbb{R}^n$, a solution $\mathbf{u}_0(t)$ is *stable* if for any bounded perturbation $\varepsilon\mathbf{v}$ such that $\mathbf{u}(t) = \mathbf{u}_0 + \varepsilon\mathbf{v}$

$$||\mathbf{u}(t) - \mathbf{u}_0(t)|| \to 0 \quad \text{as} \quad \varepsilon \to 0 \tag{1}$$

uniformly for all $t > t_0$ after some initial time t_0. A solution is *asymptotically stable* if

$$\|\mathbf{u}(t) - \mathbf{u}_0(t)\| \to 0 \quad \text{as} \quad t \to \infty \tag{2}$$

for sufficiently small $\varepsilon > 0$ [82,83]. For elastic solids, perturbations oftentimes occur in the form of free vibrations about an equilibrium solution $\mathbf{u}_0$. In this case, one has a harmonic perturbation

$$\mathbf{v}(t) = \hat{\mathbf{v}} \exp(i\omega t) \tag{3}$$

with amplitude $\hat{\mathbf{v}}$ and frequency $\omega \in \mathbb{R}$ (or, more generally, superpositions of harmonic solutions of the above form with different eigenfrequencies). Stability requires $\mathrm{Im}(\omega) \geq 0$ to avoid exponential growth of $\mathbf{v}(t)$ with time. Note that for linear elasticity, we must have $\omega \in \mathbb{R}$ for stable waves, so that instability implies $\omega^2 < 0$.

The system is in a state of (static) *equilibrium* when $\mathbf{f}(\mathbf{u}, \gamma) = 0$, which may have one or more (or no) solutions. Upon perturbation, we have

$$\frac{\partial \mathbf{f}}{\partial \mathbf{u}} \cdot \mathrm{d}\mathbf{u} + \frac{\partial \mathbf{f}}{\partial \gamma}\mathrm{d}\gamma = 0, \quad \Rightarrow \quad \frac{\partial \mathbf{u}}{\partial \gamma} = -\left(\frac{\partial \mathbf{f}}{\partial \mathbf{u}}\right)^{-1} \frac{\partial \mathbf{f}}{\partial \gamma} \tag{4}$$

which defines an *equilibrium path*. At a critical point, $\partial \mathbf{f}/\partial \mathbf{u}$ becomes singular so that there exists either no solution or a nonunique solution (point of *bifurcation*). Note that imperfections generally lower the critical point (i.e., they reduce the critical load γ) and affect the postbifurcation behavior, which is of importance both in structures (where, e.g., geometric or fabrication-induced imperfections may dominate the mechanical response) and in materials (where, e.g., thermal fluctuations lead to temperature-dependent transformation and switching kinetics).

2.2 Stability of Continuous Bodies. The previously mentioned notions of stability can be applied to discrete systems and continuous solids alike. A continuous body $\Omega \subset \mathbb{R}^d$ is described by the deformation mapping $\varphi : \Omega \times \mathbb{R} \to \mathbb{R}^d$, so that the deformed and undeformed positions, $\mathbf{x}$ and $\mathbf{X}$, respectively, are linked via $\mathbf{x} = \varphi(\mathbf{X}, t)$. Such body is governed by linear momentum balance

$$P_{iJ,J} + \rho_0 b_i = \rho_0 \frac{D^2\varphi_i}{Dt^2} \quad \text{in } \Omega \tag{5}$$

where

$$P_{iJ} = \frac{\partial W}{\partial F_{iJ}} \tag{6}$$

are the components of the first Piola-Kirchhoff stress tensor, $F_{iJ} = \varphi_{i,J}$ denotes the deformation gradient, D/Dt is the material time derivative, ρ_0 is the mass density in the reference configuration, and W is the strain energy density. Moreover, $\rho_0\mathbf{b}$ is the body force field, which is assumed to be known and independent of deformation. Here and in the following, we use index notation with Einstein's summation convention and comma indices denoting partial derivatives. Note that the above applies directly to elastic media and can also be extended to inelastic continua when using a variational formulation, see, e.g., Refs. [52] and [87].

Instabilities are often investigated in the framework of incremental deformations $\dot{\varphi}$ superimposed upon a given equilibrium state of finite deformation φ^0. Let us consider a perturbation that takes the body to a new equilibrium configuration where Eq. (5) is still satisfied and leaves the body force density unchanged. The incremental problem is governed by

$$\dot{P}_{iJ,J} = \rho_0 \frac{D^2\dot{\varphi}_i}{Dt^2} \quad \text{in } \Omega \tag{7}$$

where a dot denotes a small increment in the respective quantity caused by the perturbation. Assuming that all incremental quantities are sufficiently small (i.e., infinitesimal), the constitutive equation (6) can be linearized as

$$\dot{P}_{iJ} = \mathbb{C}^0_{iJkL}\dot{F}_{kL} \tag{8}$$

with the mixed elasticity tensor given by

$$\mathbb{C}^0_{iJkL} = \left.\frac{\partial P_{iJ}}{\partial F_{kL}}\right|_{\mathbf{F}^0} = \left.\frac{\partial^2 W}{\partial F_{iJ}\,\partial F_{kL}}\right|_{\mathbf{F}^0} \tag{9}$$

where $\mathbf{F}^0 = \mathrm{Grad}\,\boldsymbol{\varphi}^0$. Finally, we note that it is often convenient to investigate instabilities by formulating the incremental boundary value problem in an updated-Lagrangian formulation, where the reference configuration changes with time and is identified with the current configuration. In this case, the linearized form of the governing equation in the current configuration can be expressed as

$$\sigma_{ij,j} = \rho \frac{\mathrm{d}^2 u_i}{\mathrm{d}t^2} \quad \text{in } \varphi^0(\Omega) \tag{10}$$

where $\mathbf{u}: \varphi^0(\Omega) \times \mathbb{R} \to \mathbb{R}^d$ represents the incremental displacement field in the spatial description, and $\rho = \rho_0 \det \mathbf{F}$ denotes the

current density. Employing push-forward transformations based on linear momentum, one obtains

$$\sigma_{ij} = \mathbb{C}^0_{ijkl} u_{k,l} \quad \text{with} \quad \mathbb{C}^0_{ijkl} = \frac{1}{\det \mathbf{F}^0} \mathbb{C}^0_{iJkL} F^0_{jJ} F^0_{lL} \tag{11}$$

Note that in the special case of linear elastic media, the elastic moduli are independent of deformation, so that $\mathbb{C}^0 = \text{const}$ (and one often omits the superscript).

When considering the (in)stability of continuous solids, one generally differentiates between pointwise stability (which refers to material-level stability at smaller scales or localization) and structural stability (which depends on the specific macroscopic boundary value problem and corresponds to bifurcation). In the context of (in)stability in structures, analogous concepts exist for short- and long-wavelength instabilities, see, e.g., Refs. [17], [88], and [89].

2.3 Pointwise Stability. The conditions of *material stability* or *pointwise stability* are local in nature and derive from the (pointwise) governing differential equations of the medium. Consider, e.g., a solid which becomes locally unstable and localizes deformation through the formation of a discontinuity. This implies a jump in the velocity gradient field, specifically $[[\dot{\varphi}_{i,J}]] = a_i N_J$, where $\mathbf{N}$ denotes the unit normal on the plane of discontinuity, and $\mathbf{a}$ characterizes the jump. Equilibrium across the discontinuity implies that $[[\dot{P}_{iJ} N_J]] = 0$. Insertion into the incremental balance equation (8) gives the condition for localization

$$\mathbb{C}^0_{iJkL} a_i N_J N_L = 0 \tag{12}$$

for some choice of $\mathbf{a}, \mathbf{N} \neq \mathbf{0}$. Stability requires that localization does not occur for all directions, so that pointwise/material stability is ensured by

$$\mathbb{C}^0_{iJkL}(\mathbf{X}) a_i N_J a_k N_L > 0 \qquad \forall \mathbf{a}, \mathbf{N} \neq \mathbf{0} \quad \forall \mathbf{X} \in \Omega \tag{13}$$

which guarantees the *strong ellipticity* of the governing equations [90]. By van Hove's theorem, this also ensures unique (and thus stable) solutions if the entire boundary $\partial\Omega$ is rigidly constrained [91].

Alternatively, pointwise stability conditions are obtained from a linear dynamic analysis. Linear momentum balance in a linear elastic medium is governed by Eq. (7) with Eq. (8), so that one may seek separable solutions of the incremental displacement field of traveling wave form. To this end, consider the motion of a plane wave propagating at some speed c in the direction characterized by normal vector $\mathbf{N}$, so that most generally $\dot{\varphi} = \hat{\mathbf{u}} f(ct - \mathbf{N} \cdot \mathbf{X})$ with some differentiable $f : \mathbb{R} \to \mathbb{R}$. The linearized form of linear momentum balance, Eq. (7), now becomes

$$(\mathbb{C}^0_{iJkL} N_J N_L - \rho_0 c^2 \delta_{ik}) \hat{u}_k f''(ct - N_J X_J) = 0 \tag{14}$$

Consequently, real-valued wave speeds require that the acoustic tensor

$$A_{ik}(\mathbf{N}) = \mathbb{C}^0_{iJkL} N_J N_L \tag{15}$$

is positive definite for all directions $\mathbf{N} \neq \mathbf{0}$ (see, e.g., Refs. [92] and [93]), which in turn confirms the necessary, pointwise stability condition that $\mathbb{C}^0$ must be strongly elliptic, cf., Ref. 13.

For the special case of homogeneous, isotropic, linear elasticity, we have

$$\mathbb{C}^0_{ijkl} = \lambda \delta_{ij} \delta_{kl} + \mu(\delta_{ik} \delta_{jl} + \delta_{il} \delta_{jk}) \tag{16}$$

where λ and μ are the Lamé moduli; let $\kappa = \lambda + (2/3)\mu$ denote the bulk modulus in three-dimensional (3D) (for two-dimensional (2D) conditions of plane strain, we have instead $\kappa = \lambda + \mu$). The longitudinal and shear wave speeds in 3D are obtained from the eigenvalue problem (14) as, respectively,

$$c_{\text{long.}} = \sqrt{\frac{\lambda + 2\mu}{\rho_0}}, \quad c_{\text{shear}} = \sqrt{\frac{\mu}{\rho_0}} \tag{17}$$

so that strong ellipticity imposes the necessary conditions of stability (in 3D) as

$$\mu > 0 \wedge \lambda + 2\mu > 0, \quad \iff \quad \mu > 0 \wedge \kappa + \frac{4}{3}\mu > 0 \tag{18}$$

These conditions are included in the Lamé modulus map in Fig. 1. Note that the 2D (plane-strain) stability conditions can be derived analogously [94].

2.4 Global Stability. The conditions of *structural stability* or *global stability*, in contrast, are nonlocal and ensure stability of an overall body in dependence of the boundary conditions. Satisfying those guarantees that an arbitrary infinitesimal perturbation of the displacement field from an equilibrium state remains bounded for all time. The conditions of structural stability are derived from either energetic considerations, enforcing uniqueness of solutions [4,44,79,95] or from a dynamic approach that seeks to analyze the eigenmodes of a free vibration with respect to stability in the sense of Lyapunov [82].

Starting with a separable solution of the infinitesimal displacement field (with $\omega \in \mathbb{R}$ in general)

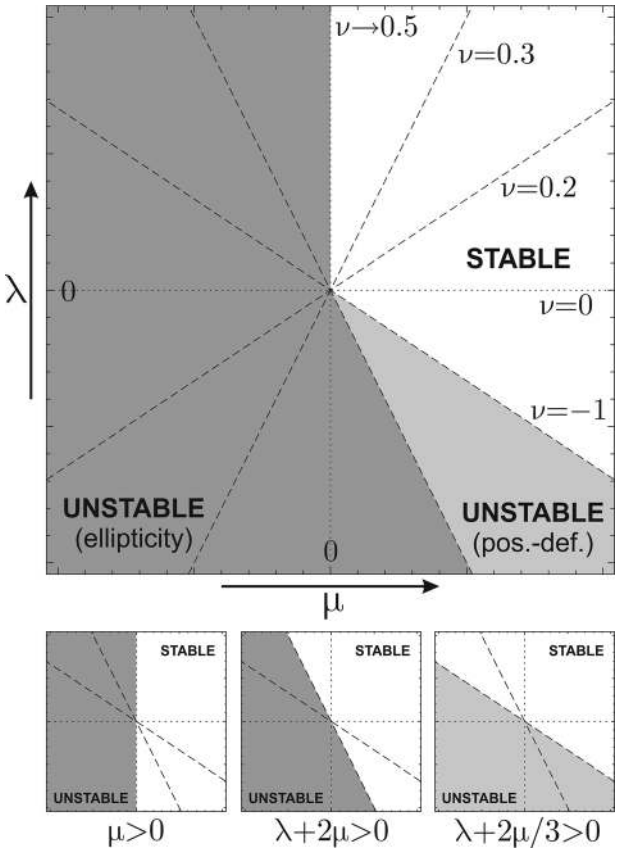

Fig. 1 Map of stable regions in the λ–μ plane of a homogeneous, isotropic, linear elastic solid. Dark-gray regions are unstable by violation of ellipticity, whereas the requirement of positive definiteness further restricts the stable region by also making the light-gray region unstable (the three key inequalities from Eqs. (18) and (23) are shown separately).

$$\mathbf{u}(\mathbf{x},t) = \hat{\mathbf{u}}(\mathbf{x})\exp(i\omega t) \tag{19}$$

linear momentum balance for a linear elastic body (or a general body in the linearized setting), Eq. (10), becomes

$$(\mathbb{C}^0_{iJkL}\hat{u}_{k,L})_{,J} + \rho_0\omega^2\hat{u}_i = 0 \tag{20}$$

Multiplication by $\hat{u}_i$, integration over Ω, and application of the divergence theorem lead to the eigenvalue problem

$$\omega^2\int_\Omega \rho_0\hat{u}_i\hat{u}_i \mathrm{d}V = \int_\Omega \hat{u}_{i,J}\mathbb{C}^0_{iJkL}\hat{u}_{k,L}\mathrm{d}V \tag{21}$$

Since the integral on the left-hand side is non-negative by definition, real-valued wave speeds (i.e., $\omega \in \mathbb{R}$ or $\omega^2 > 0$), and therefore, the stability of an elastic body requires that

$$\int_\Omega \hat{u}_{i,J}\mathbb{C}^0_{iJkL}\hat{u}_{k,L}\mathrm{d}V > 0 \tag{22}$$

For a homogeneous linear elastic body with constant moduli, positive-definiteness of $\mathbb{C}^0$ is therefore a sufficient condition of stability (which is weaker than the necessary condition of ellipticity). When introducing the concept of negative stiffness in Sec. 3.1.1, we will refer to a body with nonpositive-definite elastic moduli as one having *negative stiffness*.

For a homogeneous, isotropic, linear elastic body satisfying Eq. (16), the conditions of positive-definiteness (in 3D) reduce to

$$\mu > 0 \wedge \lambda + \frac{2}{3}\mu > 0, \quad \Longleftrightarrow \quad \mu > 0 \wedge \kappa > 0 \tag{23}$$

which are tighter than those of strong ellipticity in Eq. (18). This is illustrated in the map of Fig. 1 by the shaded regions (positive definiteness imposing tighter restrictions on the moduli than ellipticity). As shown, the isotropic moduli can also be expressed in terms of engineering measures such as Young's modulus and Poisson's ratio

$$E = \mu\frac{3\lambda + 2\mu}{\lambda + \mu} \quad \text{and} \quad \nu = \frac{\lambda}{2(\lambda + \mu)} \tag{24}$$

respectively, which yields the classical bounds $-1 < \nu < 1/2$ for positive-definiteness in 3D. Note that, if a body is rigidly constrained on its entire surface $\partial\Omega$, then ellipticity and Eq. (18) become the sufficient conditions of stability—in that case, negative Young's and bulk moduli as well as Poisson's ratios outside the above bounds can be stable, see, e.g., Refs. [94] and [96].

Equation (21) can be rearranged to yield Rayleigh's quotient, viz.,

$$\omega^2 \leq \frac{\displaystyle\int_\Omega \hat{u}_{i,J}\mathbb{C}^0_{iJkL}\hat{u}_{k,L}\mathrm{d}V}{\displaystyle\int_\Omega \rho_0\hat{u}_i\hat{u}_i\mathrm{d}V} \tag{25}$$

which bounds the lowest eigenfrequency from above. Since the denominator is by definition positive and stability of a linear elastic body again requires $\omega \in \mathbb{R}$ and thus $\omega^2 \geq 0$, the numerator must be positive for elastic stability. This ensures stability in the sense of dynamic, elastic systems.

2.5 Effective Properties. With the advancement of computational and experimental capabilities, multiscale investigations have gained importance and have linked stability to effective properties. In media with two (or more) relevant length scales, where a separation between micro- and macroscales may be assumed, homogenization techniques extract macroscale properties from representative unit cells at the microscale, see, e.g., Refs. [64] and [65]. Here, (pointwise) stability at the macroscale has been linked to structural stability at the microscale [13,62,97]. When including materials that violate elastic positive-definiteness such as in solids undergoing structural transitions, extra care is required as common assumptions of continuum elasticity theory may no longer hold [98,99].

Here and in the following, we generally refer to larger and smaller scales as *macro-* and *microscales*, irrespective of the particular length scales involved. The *effective* quasi-static macroscale properties are then defined as averages over an RVE, defining

$$\langle\cdot\rangle = \frac{1}{|\Omega|}\int_\Omega (\cdot)\mathrm{d}V \tag{26}$$

with $|\Omega|$ denoting the volume of RVE Ω.

For example, in linear elasticity, effective stress and strain tensors $\langle\boldsymbol{\sigma}\rangle$ and $\langle\boldsymbol{\varepsilon}\rangle$ are linked by an effective modulus tensor $\mathbb{C}^*$ such that $\langle\sigma_{ij}\rangle = \mathbb{C}^*_{ijkl}\langle\varepsilon_{kl}\rangle$, see Ref. [66]. In case of linear viscoelastic behavior, harmonic stress and strain fields $\boldsymbol{\sigma}(\mathbf{x},t) = \hat{\boldsymbol{\sigma}}(\mathbf{x})\exp(i\omega t)$ and $\boldsymbol{\varepsilon}(\mathbf{x},t) = \hat{\boldsymbol{\varepsilon}}(\mathbf{x})\exp(i\omega t)$, respectively, with generally complex-valued amplitudes are linked through a complex-valued effective modulus tensor $\mathbb{C}^*$ such that $\langle\hat{\sigma}_{ij}\rangle = \mathbb{C}^*_{ijkl}\langle\hat{\varepsilon}_{kl}\rangle$, see Refs. [100] and [101]. For particular loading scenarios, one can characterize the effective material *damping* by the loss tangent $\tan\delta$, defined by the phase lag δ in the time domain. For example, for uniaxial loading, we have $\varepsilon(t) = \hat{\varepsilon}(t)\exp(i\omega t)$ and $\sigma(t) = \hat{\sigma}\exp(i(\omega t - \delta))$. In case of nonlinear material behavior, the effective response depends on deformation and, e.g., the effective incremental modulus tensor is given by

$$\mathbb{C}^{0*}_{iJkL} = \left.\frac{\partial\langle P_{iJ}\rangle}{\partial\langle F_{kL}\rangle}\right|_{\langle\mathbf{F}\rangle=\mathbf{F}_0} \tag{27}$$

Other effective properties can be defined analogously.

3 Exploiting Instabilities in Solids and Structures

As pointed out earlier, both local and global instabilities may occur in solids and structures. In recent years, both of them have been exploited to produce interesting, peculiar, extreme, or beneficial macroscopic material behavior. Most such concepts can be grouped into two categories to be explained in great detail in Secs. 3.1 and 3.2. Section 3.1 focuses on using the loss of positive-definiteness (often referred to as *negative stiffness*) as a material property. While unstable in a free-standing solid, we will discuss how nonpositive-definite phases can be stabilized in a composite and how such stable negative stiffness is utilized to control the effective, overall composite properties. By contrast, Sec. 3.2 reviews examples in which (i) structural instabilities are exploited to induce large deformations that enable the control and tuning of the effective properties of the system (without necessarily using nonpositive-definite constituents) and (ii) the rather recent concept of utilizing instability to propel stable, large-amplitude nonlinear wave motion.

3.1 Negative Stiffness and Material Instability

3.1.1 The Concept of Negative Stiffness. The strategy of exploiting so-called *negative-stiffness* components in structures and solids is based on a simple yet powerful idea. Most engineering design principles achieve target material properties by combining constituents which—individually or jointly—contribute the properties of interest. For example, combining a lossy viscoelastic material with a stiff elastic material can result in composites offering both stiffness (i.e., the ability to carry loads) and damping (i.e., the ability to absorb vibrational energy) [102–105]. In the

design of such composite systems, one commonly works with constituents having positive definite-elastic moduli—this ensures stability of each phase under arbitrary boundary conditions. A key observation was that the geometric constraints between the various phases in a composite provide a means of stabilization, so that phases with nonpositive-definite elastic moduli (phases having *negative stiffness*) may, in principle, exist and be stable if constrained. In other words, while a homogeneous linear elastic medium must have positive-definite moduli for stability under general boundary conditions, a composite may not necessarily require all of its constituents to satisfy positive-definiteness for stability. This led to a careful analysis of both stability and effective properties of such composites containing negative-stiffness phases. The full analysis of multiphase composites is mathematically involved, which is why—before analyzing complex, higher-dimensional composite materials—we first turn to mass–dashpot–spring systems as simple structural analogs that admit intuitive, closed-form solutions. In fact, spring systems have been used early on to study the presence of negative-stiffness phases, see, e.g., Ref. [106]. While the loss of stability in solids is linked to checking the above local and global conditions imposed upon the components of the incremental stiffness tensor, the stability of a spring is simply linked to the sign of its scalar stiffness. Composites, difficult to deal with in 2D/3D, in general, because of geometric effects and complex boundary conditions, are easily assembled by multiple springs in one-dimensional (1D)—like the classical Reuss and Voigt composites. Even the transition from elastic to viscoelastic composites can be discussed by adding dashpots to the spring analogs (while requiring more complex tensorial counterparts in higher-dimensional systems). For all those reasons, we introduce the basic concepts of negative stiffness, multistability, and effective properties by simple spring examples.

3.1.2 Springs as Structural Analogs. Structural instability emerges, e.g., in a bistable system (i.e., a structure having two stable equilibrium configurations which correspond to two local energy minima). If the energy potential is continuous, then there must also be local energy maximum which corresponds to an unstable state.

Consider, e.g., the mass–spring toy example shown in Fig. 2(*a*). The system consists of two linear elastic springs of stiffness k and a point mass m which is assumed to move only horizontally. The mass has two stable equilibrium positions at $x = \pm l$, corresponding to two energy minima, while the central position $x = 0$ corresponds to a local maximum (hence, an unstable equilibrium), as shown by the total potential energy E plotted in Fig. 2(*c*). This is as a prototype of a *bistable* elastic system. The potential energy landscape is inherently nonconvex, which comes with nonlinearity in the physical constitutive behavior since $F = \partial E/\partial x$. Displacement-controlled loading here results in a nonmonotonous force–displacement relation, whereas load control leads to snapping from one equilibrium branch to another.

Since we restrict the mass' motion to be horizontal, the effective static stiffness k_a^* of the overall system depends nonlinearly on the mass' position x via

$$k_a^*(x) = \frac{\partial^2 E}{\partial x^2} = 2k\left(1 - \frac{h^2\sqrt{h^2 + l^2}}{(h^2 + x^2)^{3/2}}\right) \tag{28}$$

see Fig. 2(*a*) for the definition of the geometric parameters. Therefore, negative effective stiffness, $k_a^* < 0$, occurs when

$$-\sqrt{(h^4(h^2 + l^2) - h^2)^{1/3}} < x < \sqrt{(h^4(h^2 + l^2) - h^2)^{1/3}} \tag{29}$$

but is unstable in an unconstrained system (under load control, the mass will snap through the unstable, concave region of E in Fig. 2(*c*)).

As an extension, the composite system shown in Fig. 2(*b*) adds in series another linear spring of constant stiffness $k_2 > 0$. Imagine the application of a force F^0, resulting in a position x^0 of the (left) mass in the composite system. Assuming that the system is stable in that configuration, we may linearize about x^0 with respect to small perturbations in the load and displacement. The resulting system with incremental load–displacement relation $\dot{F} = k^*\dot{x}$ is visualized in Fig. 2(*d*), where we redefined $k_1 = k_a^*$ for simplicity, and it yields the effective static stiffness

$$k^* = \frac{k_1 k_2}{k_1 + k_2} \tag{30}$$

Stability requires $k^* \geq 0$ so that (assuming $k_2 > 0$), we must also have

$$k_1 \geq 0 \tag{31}$$

for stability under general boundary conditions (any $k_1 < 0$ is unstable under load control). Note that if we add a third spring

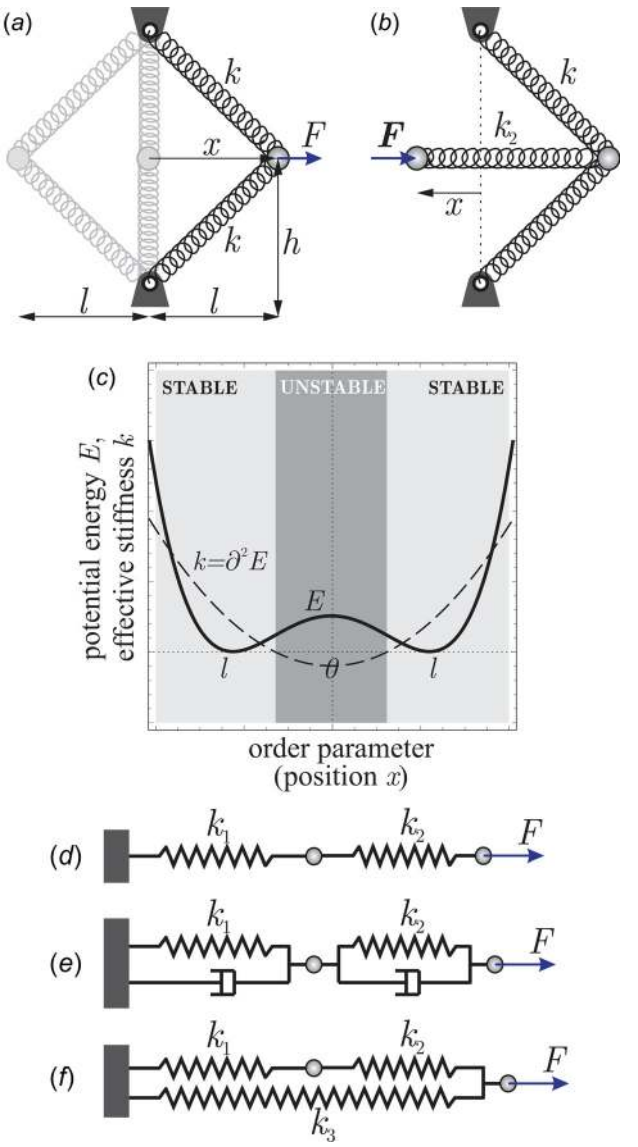

Fig. 2 Simple spring examples: (*a*) bistable mechanical system and (*b*) composite spring system; the energy and stiffness of system (*a*) is illustrated in (*c*); (*d*) linear spring reduction of system (*b*) where $k_1 = k_a^*$ and (*e*) its viscoelastic extension; (*f*) composite system

with stiffness $k_3 > 0$ in parallel to the other two springs, see Fig. 2(*f*), then the effective stiffness becomes

$$k^* = k_3 + \frac{k_1 k_2}{k_1 + k_2} \tag{32}$$

in which case stability requires

$$k_1 \geq k_{1,\text{crit}} = -\frac{k_2 k_3}{k_2 + k_3} \tag{33}$$

That is, for $k_2, k_3 > 0$ negative values of k_1 can indeed be stable under general loading. Apparently, infinite effective stiffness $k^* \to \infty$ is predicted for $k_1 \to -k_2$ from below, but this is necessarily unstable because $k_1 \geq k_{1,\text{crit}} > -k_2$ unless $k_3 \to \infty$ (in which case, the system is infinitely stiff anyways). Note that negative values of k_1 can serve to create systems with very low effective stiffness k^*, which may be of interest for controlling the resonance frequencies of the system [107].

It is important to note that we here refer to the positive or negative *static* stiffness of the elastic system or its components, which should not be confused with the effective *dynamic* stiffness which has also been tuned to negative values in acoustic metamaterials exploiting, e.g., local resonators [108–110]. In our case, negative stiffness refers to the quasi-static load–displacement relation and is tied to the release of internal energy (such as energy release upon snapping of the bistable spring system).

Finally, consider the viscoelastic system obtained from replacing the elastic springs by viscoelastic spring–dashpot combinations, see Fig. 2(*e*). In case of linear dashpots (i.e., velocity-proportional damping) with viscosities $\eta_i > 0$, the effective complex-valued *quasi-static* stiffness of the simple composite under harmonic excitation with frequency ω (inertial effects are neglected) is by the correspondence principle [100]

$$k^* = \frac{k_1^* k_2^*}{k_1^* + k_2^*} \tag{34}$$

with

$$k_j^* = k_j + i\omega\eta_j \tag{35}$$

The resulting effective stiffness (assuming $k_2 > 0$) is

$$|k^*| = \sqrt{\text{Im}(k^*)^2 + \text{Re}(k^*)^2} = \sqrt{\frac{\left(\eta_1^2\omega^2 + k_1^2\right)\left(\eta_2^2\omega^2 + k_2^2\right)}{\omega^2(\eta_1 + \eta_2)^2 + (k_1 + k_2)^2}} \tag{36}$$

and the effective damping is characterized by

$$\tan\delta = \frac{\text{Im}(k^*)}{\text{Re}(k^*)} = \omega\frac{\eta_2 k_1^2 + \eta_1 k_2^2 + \eta_2\left(\eta_1\omega^2(\eta_1 + \eta_2)\right)}{\omega^2\left(\eta_2^2 k_1 + \eta_1^2 k_2\right) + k_1 k_2(k_1 + k_2)} \tag{37}$$

Figure 3 illustrates the effective stiffness and damping and demonstrates the impact of negative values of k_1 (assuming $k_2 > 0$). Recall that stability requires (31) (which remains unaffected by the addition of viscosity). Results in Fig. 3 indicate that, as k_1 approaches the stability limit ($k_1 \to 0$ from above), significant increases in damping can be achieved, while the effective stiffness is reduced considerably. The same was shown for more complex two-phase composites consisting of negative-stiffness inclusions embedded in a stabilizing matrix phase [101]. Note that these analyses ignore inertial effects, which can easily be added and provide altered results that also depend on the masses and may produce local resonance effects [107].

The previously mentioned concept of utilizing mechanical systems near instability to create an effective negative stiffness was first utilized in structures, e.g., for vibration isolation [29,111].

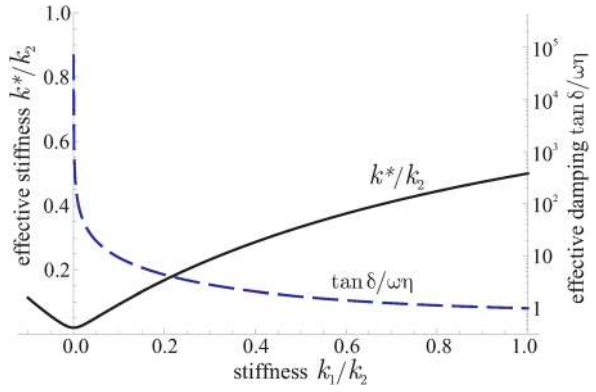

Fig. 3 Effective (normalized) stiffness and damping of the linear viscoelastic composite system of Fig. 2(*e*) versus (normalized) spring stiffness k_1 (shown for $\eta\omega = 0.01$ and $k_2 > 0$)

Constrained snap-through instabilities in precompressed, buckled beams (as a more practical implementation of the scenario in Fig. 2(*a*)) were used to reduce the stiffness of elastic suspensions and to achieve low natural frequencies, see also Ref. [31]. Applications ranged from vibration isolation for nano-instrumentation [112] to vibration reduction in vehicles [113] and structures [32], to seismic protection technologies [114]. Negative incremental stiffness has also been reported in foams [115] and structures with interlocked elements [116]. Further examples of structures exploiting constrained bistable, negative-stiffness elements can be found in Refs. [117–120] with nonlinear extensions in Ref. [121]. The concept of operating a stabilized mechanical system close to a critical point had also been found in biological systems such as myofibrils [122], muscles [123], and hair cell walls [124], where—among others—the high, controllable sensitivity near the critical point is exploited.

At the material level, negative stiffness implies nonpositive-definite (incremental) elastic moduli $\mathbb{C}$, which may result from constrained material instabilities (e.g., from phase transformations). For example, the potential energy of materials undergoing second-order phase transformations is often described by Landau's theory [46]: having only a single well at high temperature, the potential energy turns into a multiwelled landscape below the transformation temperature. Upon cooling through the transition temperature, the initially stable high-temperature energy minimum turns into a local maximum below the transformation point which becomes unstable but, if sufficiently constrained, may be stabilized to display nonpositive-definite moduli [40].

Early approaches to take advantage of the negative-stiffness concept in materials were based on theoretical predictions of stiffness and damping in composites. For example, by evaluating the property bounds of Hashin–Shtrikman composites [125], nonpositive-definite phases were shown to produce extreme viscoelastic properties [38]. Similar to later predictions based on fractal composite models [126], those investigations predicted extreme variations in the composite's effective stiffness and damping due to the presence of negative-stiffness phases (where the term *extreme* stands for effective properties that surpass those of each constituent).

As an example, Fig. 4 illustrates the effective dynamic Young's modulus and the effective damping obtained from evaluating the Hashin–Shtrikman lower bound for a composite composed of a metal matrix (with moduli $\mu_{\text{mat}} = 19.2$ GPa, $\kappa_{\text{mat}} = 41.6$ GPa, and three values of $\tan\delta = 0.01$, 0.02, and 0.04) with 5 vol % ceramic inclusions ($\mu_{\text{inc}} = 50$ GPa and $\tan\delta = 0.001$) whose bulk modulus κ_{inc} is varied from positive to negative values. For $\kappa_{\text{inc}} > 0$, the few inclusions have little impact on the effective response. For $\kappa_{\text{inc}} \approx -24$ GPa, strong variations in Young's modulus and loss tangent are predicted (these are even more remarkable as only 5 vol % inclusions are responsible for the shown

changes in the overall properties). As shown later in Refs. [127] and [128], composite bounds also predicted the piezo-, pyro-, or thermomechanical coupling coefficients to assume extreme values in particulate composites with negative-stiffness inclusions in a viscoelastic matrix, similar to Fig. 4. Composites were further shown to serve as waveguides with exceptional damping due to negative-stiffness phases [129].

The combination of high stiffness and high damping is of particular technological interest as those properties are naturally exclusive [130], owing to the distinct responsible microscale mechanisms (high stiffness favors perfect crystallinity, whereas high damping requires high mobility of defects or related mechanisms of internal friction). In fact, plotting the stiffness versus damping of many natural and manmade materials (see Fig. 5) revealed a seemingly natural upper bound on the combined figure of merit of stiffness times damping, $E \times \tan\delta$, for all known materials [131]; the region of high stiffness and damping in Fig. 5 remained empty. The negative-stiffness strategy offered opportunities to achieve composites having both high stiffness and high damping (with optimal combinations sought, e.g., via topology optimization [132]), which can enter the empty parameter range, as discussed in Secs. 3.1.3 and 3.1.4.

3.1.3 Composite Materials: Theoretical Studies. Following those early estimates based on composite bounds, more theoretical studies of specific composites followed with the aim to contrast extreme property predictions with stability restrictions. After all, the question had remained whether or not extreme composite properties due to negative-stiffness phases could be stable under general loading/boundary conditions.

Coated cylinders and spheres are prototypical examples of two-phase composite bodies with Lamé-type solutions in small strains. A first continuum-mechanics analysis of both 2D and 3D configurations (i.e., coated cylinders and spheres) showed that negative stiffness in the inclusion may indeed lead to extreme overall increases in the overall bulk modulus in case of linear and nonlinear elastic composites [133]. Dynamic stability analysis using the same two-phase composite bodies within linear elasticity further revealed that nonpositive-definite inclusions can indeed be stable if sufficiently constrained, e.g., when embedded in a stiff coating or matrix [98,134]. Specifically, for homogeneous, isotropic linear elastic phases, it was shown that a negative inclusion bulk modulus can be stable if the surrounding coating is sufficiently stiff and thick.

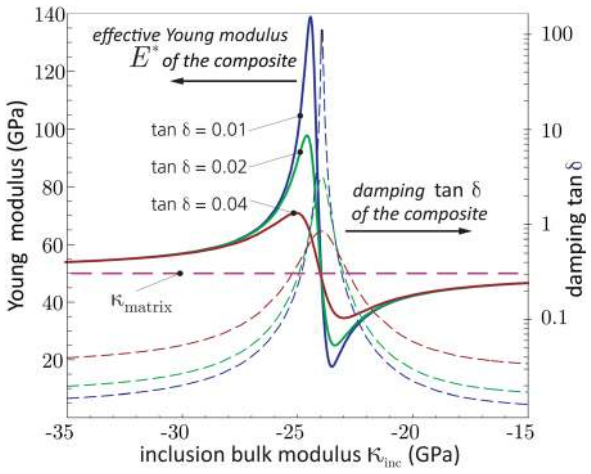

Fig. 4 Effective viscoelastic Young's modulus and loss tangent for a Hashin–Shtrikman composite composed of metal matrix ($\mu_{mat} = 19.2$ GPa, $\kappa_{mat} = 41.6$ GPa, and three values of $\tan\delta = 0.01, 0.02$, and 0.04) and 5 vol % ceramic inclusions ($\mu_{inc} = 50$ GPa, $\tan\delta = 0.001$, and varying κ_{inc}). The shown effective modulus refers to the absolute value of the complex-valued viscoelastic Young's modulus $E^* = E_{re} + iE_{im}$.

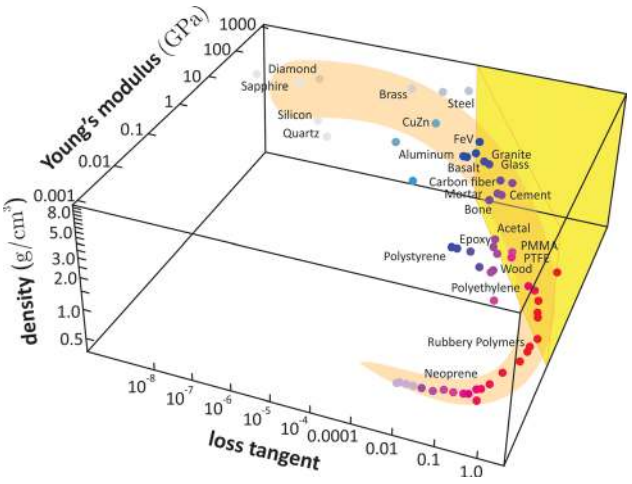

Fig. 5 Stiffness (Young's modulus) versus damping (loss tangent) versus mass density for a variety of natural and manmade materials; the shadowed prism highlights the desirable but challenging region of combined high stiffness and high damping

The global stability conditions were derived in the two ways described in Sec. 2. As shown in Ref. [98], one can solve the dynamic, linear elastic eigenvalue problem for macroscopic bodies Ω to determine the infinite set of eigenfrequencies (or at least the lowest few). That is, one solves Eq. (20) with suitable boundary conditions (e.g., pure traction boundary conditions over $\partial\Omega$ as the weakest constraint) for the eigenfrequencies ω_i. For linear elastic bodies, stability requires that $\omega_i \in \mathbb{R}$. Therefore, once the lowest nonzero eigenfrequency ω_0 is known as a function of elastic moduli and geometry, stability conditions on the elastic moduli can be established. Alternatively, stability conditions were derived by evaluating Eq. (22) for specific composite geometries [134]. Furthermore, by exploiting Rayleigh's coefficient (25), finite element analysis was conveniently used as an inexpensive alternative [94] (which requires checking the positive-definiteness of the global stiffness matrix). As could be expected for conservative systems (such as linear elastic media), all the three approaches led to the same conclusion, viz., that nonpositive-definite inclusion phases can be stable if sufficiently constrained. For example, Fig. 6 shows the stable and unstable moduli combinations for the shown coated-sphere two-phase body as light and dark regions, respectively, clearly indicating that the inclusion's bulk modulus, κ^i, can be negative and stable if the coating's bulk modulus, κ^c, is sufficiently high [107].

For conservative linear systems, one can exploit the equivalence of static and dynamic stability, following Hill [79] and Koiter [84], which led to simplified stability analyses. For example, for rotational-symmetric bodies such as coated cylinders or coated spheres, the lowest (nonzero) eigenfrequency typically corresponds to a rotational-symmetric deformation mode and is therefore linked to the effective bulk modulus of the two-phase body [96]. Therefore, the stability limit can alternatively be obtained by computing $\langle\kappa\rangle$ as a function of constituent moduli and geometry and enforcing $\langle\kappa\rangle \geq 0$ for stability (in close analogy to the spring example of Sec. 3.1.1). Based on this approach, new closed-form stability bounds were derived for 2D and 3D composite bodies [96].

Finally, an alternative protocol was proposed in Ref. [135] to derive closed-form stability bounds: by exploiting the uniqueness of solutions in linear elasticity, the static boundary value problem is solved and instability is linked to the existence of nontrivial solutions. Using this approach, an expanded stability regime was reported for composites with multiple positive/negative-stiffness phases [135].

It is important to note that all of the aforementioned stability analyses were concerned with deriving the structural or global

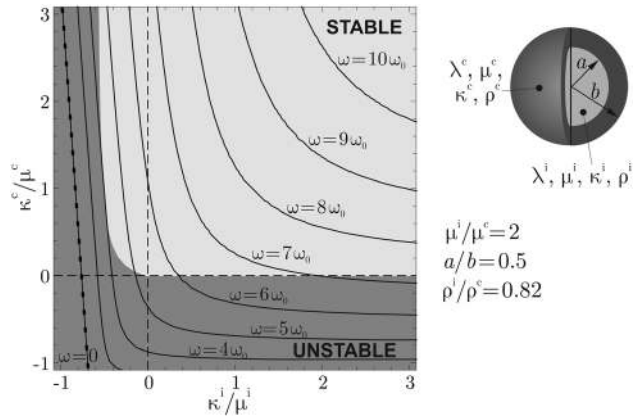

Fig. 6 Stable and unstable moduli combinations for a coated spherical inclusion (stable and unstable combinations are shown as light and dark gray regions, respectively); both phases are homogeneous, isotropic, linear elastic (with $\mu^c, \mu^i > 0$ for pointwise stability). Under static conditions, an infinite effective bulk modulus of the two-phase body is unstable (shown by the $\omega = 0$ line are all moduli combinations resulting in a positive-infinite bulk modulus). Under dynamic excitation, resonance effects lead to strong stiffness variations which, with increasing excitation frequency ω shift in to the stable region ($\omega_0 = \sqrt{\mu^c/\rho^c b}$). When admitting negative stiffness $\kappa^i < 0$, these become stable at significantly lower frequencies [107].

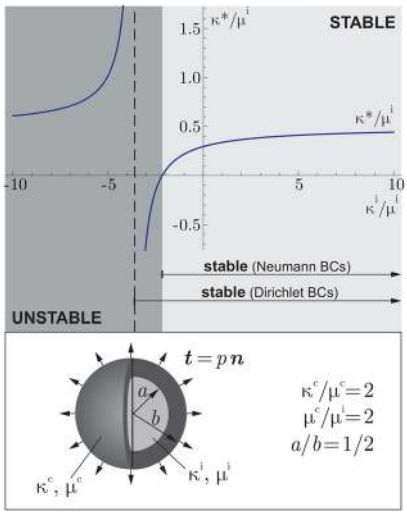

Fig. 7 Stability map showing stable (light) and unstable (dark gray) regions of κ^i/μ^i, where κ^i and μ^i are, respectively, the bulk and shear moduli of a spherical inclusion (radius *a*) embedded in a concentric coating (outer radius *b* and moduli κ^c, μ^c). The stability limit for κ^i/μ^i depends on the applied BCs. Plotted is the effective bulk modulus $\kappa^* = pb/3u_r(b)$ for uniform applied pressure *p*, resulting in a rotational-symmetric expansion of the coated-sphere composite with radial displacement field $u_r(r)$. Consequently, under both types of BCs, the solid loses stability before the effective modulus tends to $+\infty$ with decreasing κ^i/μ^i. Note that positive-definiteness corresponds to $\kappa/\mu \geq 0$, so that the elastic coating expands the stable regime of the inclusion phase.

conditions of stability. Independently, every composite constituent must locally satisfy the necessary conditions of stability, viz., the strong ellipticity of the elastic modulus tensors (which is equivalent to positive-definiteness of the acoustic tensor in Eq. (15)). The sufficient conditions of stability thus result from the satisfaction of both local and global stability constraints for any given composite.

Now that detailed stability conditions and effective property calculations were available for 2D and 3D composite examples, a comparison of both unfortunately revealed that linear elastic composites with negative-stiffness phases cannot produce stable extreme effective stiffness [107,136], because the composite loses stability before the negative-stiffness phase can lead to extreme stiffness increases, see, e.g., the stable region in Fig. 6 and the line labeled $\omega = 0$ which indicates moduli combinations leading to extreme (i.e., positive infinite) overall stiffness under static conditions. This was confirmed by rigorous bounds derived for multiphase linear elastic composites with nonpositive-definite phases. In particular, it was shown that the Voigt bound for general composites as well as the Hashin–Shtrikman bound for isotropic composites can be reinterpreted as stability conditions. Exceeding those bounds (which is required for extreme overall stiffness) renders the composite necessarily unstable [99]. Figure 7 shows an example that the effective bulk modulus κ^* of a coated spherical inclusion (whose bulk modulus κ^i is assumed to become negative) shows extreme variations but only for negative values of the inclusion bulk modulus beyond the stability limit, both for rigid-displacement and general boundary conditions (Dirichlet and Neumann problems, respectively). The former adds some stabilization as can be seen by the shifted stability limit, but that stabilization is insufficient to allow for stable extreme bulk stiffness $\kappa^* \to +\infty$. Based on the aforementioned link between composite bounds and stability limits, this conclusion can be generalized to other elastic moduli including those of anisotropic solids.

In contrast to the elastic stiffness, extreme viscoelastic damping was shown to be theoretically stable, like in the simple spring example of Sec. 3.1.1. Discrete spring–mass–dashpot structures played a central role in early studies deriving effective viscoelastic properties and stability without the need for a full continuum analysis, see, e.g., Refs. [137–141]. These studies confirmed that, although extreme composite damping (and compliance) can be achieved, extreme stiffness cannot be stable [106]. For linear viscoelastic solids, stable extreme damping was derived for two-phase composites [142], see also Ref. [143] and the numerical confirmation by finite elements in Ref. [144]. Multiscale simulations of viscoelastic composites with negative-bulk-modulus inclusions [101] and with phase-transforming inclusions [145], in both cases embedded in a viscoelastic matrix material, confirmed that extreme increases in the composite's effective damping capacity under dynamic excitation can be stable.

Since viscoelastic experiments using time-harmonic loading had revealed extreme properties (including extreme damping), further stabilization was sought from dynamic loading. Similar to the vibration of an inverted pendulum [146,147], the dynamic excitation of composites was shown to expand the stable regime. Here, the effect of nonconservative forces plays an important role, e.g., by spinning a composite at sufficiently high frequency, gyroscopic forces can provide stabilization, as shown for both continuum composites at the example of a coated cylinder [85] and for discrete mass–spring systems [148]. For the latter, it was shown that even extreme stiffness can be stabilized by the gyroscopic forces. Further stabilization was reported in nonequilibrium systems with energy flux [149].

The influence of inertial effects in two-phase solids was investigated in Ref. [107] and showed that the presence of a nonpositive-definite phase can significantly reduce the spectrum of resonant frequencies, resulting in strong stiffness variations due to resonance. The solid lines in Fig. 6 illustrate modulus combinations leading to extreme effective *dynamic* stiffness of the composite (considering the action of inertia) at different excitation frequencies ω, i.e., the loading is as the same as in Fig. 7 but with $p(t) = \hat{p}\exp(i\omega t)$ resulting in the effective *dynamic* bulk modulus $\kappa^* = \hat{p}b/3\hat{u}_r(b)$. For an elastic solid, those lines correspond to positive-infinite stiffness; for a viscoelastic solid, the effective stiffness would be bounded but high. Results in Fig. 6 show how the predicted strong stiffness increases shift into the stable region of moduli combinations with increasing excitation frequency.

3.1.4 Composite Materials: Experimental Studies. Although we discussed theoretical and numerical studies first, experimental research was underway at the same time and has fueled the former by giving insight into the effective behavior of systems with constrained negative-stiffness constituents. Experiments also provided evidence that interesting properties could be attained in this fashion.

Beginning with structural instabilities, experiments on composite structures such as postbuckled, embedded silicone rubber tubes indeed showed significant damping peaks [37] with maximum damping observed orders of magnitude in excess of the damping of pure silicone rubber. Similarly, buckling was later utilized in carbon-nanotube composites [30], where applied compression brought the nanotubes near their critical points.

At the material level, most experiments used phase transformations in solids to induce nonpositive-definite phases: when embedded in a stiff matrix, phase-transforming inclusions are geometrically constrained and the delayed phase transformation may result in temporarily stable negative stiffness in the inclusion phase. Probably the first example, VO_2 inclusions embedded in a tin matrix displayed extreme damping and large variations in stiffness due to the phase transformation in the inclusion phase [39]. Figure 8 illustrates the viscoelastic compliance and damping measured in torsion at 100 Hz. Experiments on composites with VO_2 particulate inclusions showed that extreme properties could indeed be achieved with low VO_2 concentrations (below 5 vol %) but that this no longer applied at higher concentrations [150,151] due to a reduction in stabilization.

As a further example, Sn–$BaTiO_3$ composites showed extreme viscoelastic stiffness and damping variations under time-harmonic bending [40], as shown in Fig. 9. Like in the VO_2 example, temperature was used to control the phase transformation, and measured data showed varied responses with increasing numbers of thermal cycles. This effect was primarily attributed to the progressive weakening of particle-matrix bonding, failure and damage mechanisms, as well as accumulating plastic strains surrounding the inclusions (see Ref. [145] for a computational analysis showing damage and degradation surrounding the inclusion phase). Experiments on indium–thallium alloys showed damping peaks and sigmoid-shaped anomalies in the shear modulus at high cooling rates due to the temperature-induced martensitic transformation [152], which was also attributed to constrained negative stiffness. Further experiments were reported for $BaZrO_3$–ZnO [153] and $Zn_{80}Al_{20}$–$BaTiO_3$ [154]. In many of the aforementioned ferroelectric perovskite inclusions, the negative-stiffness mechanisms were theoretically associated with an oxygen vacancy mechanism [153].

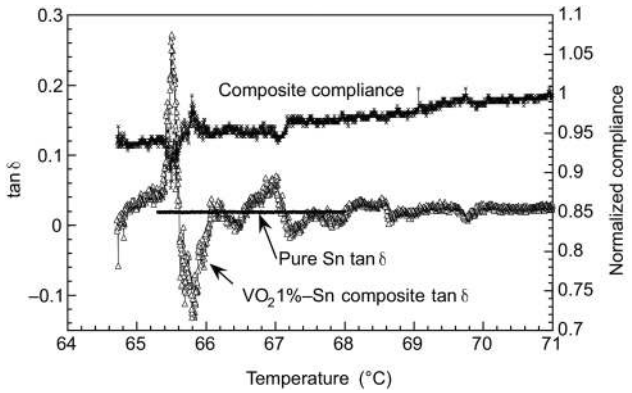

Fig. 8 Torsional compliance (inverse stiffness) and loss tangent versus temperature of a composite composed of 1 vol % VO_2 particles embedded in a pure tin matrix (damping of pure tin is included for reference). Measurements were conducted well below sample resonance at 100 Hz. Reprinted with permission from Lakes et al. [39]. Copyright 2001 by Nature Publishing Group.

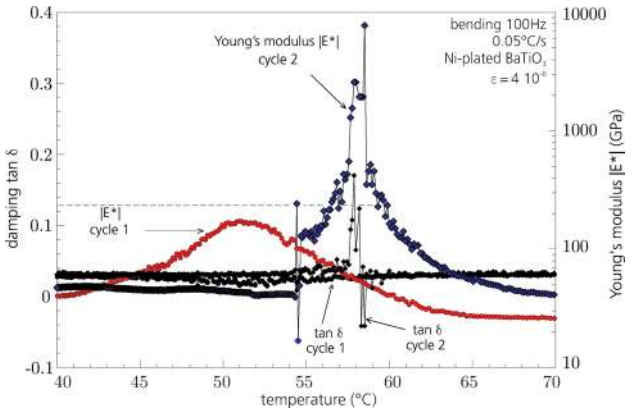

Fig. 9 Dynamic stiffness and damping variations in viscoelastic Sn–$BaTiO_3$ composites under harmonic loading. Adapted from Ref. [40].

Experiments on unconstrained phase-transforming materials demonstrated strong variations in the (visco)elastic moduli during the ferroelastic transition of, e.g., $BaZrO_3$–$BaTiO_3$ [155] (shown were variations in Poisson's ratio and the effective bulk modulus). In unconstrained samples, the transformation was shown to result in pronounced softening. However, such stiffness reduction during the transformation could at most reach zero stiffness (and not display negative stiffness) in an unconstrained sample. It was theorized that in a constrained system (such as particles embedded in a matrix), negative stiffness can be stabilized as derived theoretically [96,98,107,134]. Negative stiffness was detected in unconstrained phases by special nanoindentation techniques [156], and it was also reported in phase-transforming systems such as ZrW_2O_8 during a ferroelastic cubic-orthorhombic pressure-induced phase transition [157]. Ferroelectric switching in perovskite ceramics is another mechanism that induces instability (by applied electric fields). The resulting variations in stiffness and damping were measured, e.g., for lead zirconate titanate where a strong viscoelastic softening was observed during the switching process [42,158].

It is important to note that all of those material-level experiments characterized the *dynamic* (visco)elastic moduli and demonstrated extreme increases in the effective damping and significant variations in the effective stiffness (some stiffness variations reaching extreme values orders of magnitude above those of the constituent materials). By contrast, theory showed that the classical upper composite bounds on the elastic moduli presented stability conditions [99], implying that negative-stiffness constituents (even though possibly stable when embedded in a stiff matrix) can never lead to a composite performance surpassing the stiffness of individual constituents. Those theoretical conclusions, however, applied to the *quasi-static* elastic moduli and, as mentioned earlier, theoretical/numerical studies indeed revealed the potential for extreme damping and stiffness in dynamically excited solids and the importance of potential resonant effects [107]. Even though experiments were generally designed to operate far below the first specimen resonance, this did not necessarily account for the specimen stiffness decreasing significantly as a consequence of the phase transformation in the inclusion phase [107], as described in Fig. 6. The full range of opportunities in exploiting instability in the dynamic setting still poses many questions and fuels ongoing research.

3.2 Structural Instability and Metamaterials

3.2.1 Instability-Driven Pattern Formation. Periodic and porous structures made of elastic materials such as elastomers and gels undergo significant and reversible deformation in response to diverse stimuli, including mechanical loading, swelling, and

changes in temperature and electric signals. When excessive deformation is applied, they may eventually become unstable. Beyond the instability threshold, rapid and dramatic changes of the structural geometry occur, and a careful design of the initial architecture may lead to the formation of new and homogeneous periodic patterns [159–162]. Interestingly, it has been recently shown that such dramatic geometric rearrangements induced by instabilities can be exploited to rapidly tune the macroscopic response and functionalities of the structures [22,34,163–174].

The recent developments in the field have been enabled by the convergence of advances in computational tools and experimental techniques, which now make it possible to easily simulate and fabricate structures of complex form. Experimentally, recent advances in digital fabrication have enabled manufacturing of systems with arbitrary shapes across length scales and made out of a wide ranges of materials, facilitating the exploration of the design space [175]. On the computational side, to reduce the time and make sure the behavior of the systems is not dominated by boundary effects, most of the studies have focused on infinite periodic systems, considering unit cells with appropriate boundary conditions. Despite the fact that instabilities often alter the periodicity of the structure, buckling can be still studied on the initial unit cell by investigating the propagation of small-amplitude waves of arbitrary wavelength superimposed on a state of finite deformation [162,176–179]. Specifically, the onset of buckling corresponds to the first point along the loading path for which a wave with vanishing natural frequency exists (assuming that rigid-body modes are suppressed).

To conduct such analysis, the unit cell is first subjected to a state of finite deformation φ^0. Then, the propagation of small-amplitude elastic waves in the predeformed cell is investigated by applying Bloch-type boundary conditions [68]

$$\mathbf{u}(\mathbf{x},t) = \hat{\mathbf{u}}(\mathbf{x})e^{i(\mathbf{k}\cdot\mathbf{x}-\omega t)} \tag{38}$$

where $\hat{\mathbf{u}}(\mathbf{x})$ satisfies the periodicity of the underlying lattice and ω is the frequency. Moreover, $\mathbf{k}$ denotes the wave vector

$$\mathbf{k} = \frac{\mathbf{b}_1}{m_1} + \frac{\mathbf{b}_2}{m_2} + \frac{\mathbf{b}_3}{m_3} \tag{39}$$

where m_i ($I = 1, 2, 3$) are the numbers of unit cells contained in a full wavelength along the direction of the ith lattice vector, and $\mathbf{b}_i$ are the reciprocal primitive vectors defined as

$$\mathbf{b}_1 = 2\pi\frac{\mathbf{a}_2\times\mathbf{a}_3}{||\mathbf{z}||^2}$$
$$\mathbf{b}_2 = 2\pi\frac{\mathbf{a}_3\times\mathbf{a}_1}{||\mathbf{z}||^2} \tag{40}$$
$$\mathbf{b}_3 = 2\pi\frac{\mathbf{a}_1\times\mathbf{a}_2}{||\mathbf{z}||^2}$$

$\mathbf{a}_i$ being the lattice vectors spanning the unit cell and $\mathbf{z} = \mathbf{a}_1\cdot(\mathbf{a}_1\times\mathbf{a}_2)$. Substitution of Eq. (38) into Eq. (10) leads to the eigenvalue problem

$$[-\mathbb{C}^0_{ijkl}k_j + i\,\mathbb{C}^0_{ijkl,j}]k_l\hat{u}_k - \rho\omega^2\hat{u}_i = 0 \tag{41}$$

to be solved over the continuous body Ω for different combinations of m_1, m_2, and m_3. An instability is detected at the lowest value of applied deformation for which m_1, m_2, and m_3 exist such that the corresponding wave has vanishing frequency ω.

One of the simplest examples of instability-driven pattern formation in elastic metamaterials is that observed in a square array of circular holes in a 2D elastomeric matrix. Bloch wave stability calculations first showed that for such structure, a microscopic bifurcation instability occurs before the macroscopic loss of ellipticity, resulting in an antisymmetric bifurcation mode characterized by a pattern of alternating, mutually orthogonal ellipses [162] (see Fig. 10(*a*)). These predictions have then been confirmed by experiments [159,160] (see Fig. 10(*b*)). Note that this metamaterial can be seen as an array of rigid domains (gray squares in Fig. 10(*b*)) connected by beamlike thin ligaments (green lines in Fig. 10(*b*)). Each beam buckles into the energetically most favored configuration—a half-sinusoid—and induces rotation of the rigid domains, resulting in the formation of a pattern of mutually orthogonal ellipses.

Building on these initial results, a library of 2D [21,174,180,181] and 3D [164] porous structures and structured porous shells [22,169,182] in which buckling induces pattern transformations has been identified (see Fig. 11). Moreover, while in most of the cases mechanical loading is used to deform the structures and trigger the instabilities, it has also been shown that other stimuli including swelling [160,165–168,183] (see Fig. 12(*a*)), capillary pressure [172] (see Fig. 12(*b*)) and magnetic fields [184] (see Fig. 12(*c*)) can result in instability-driven pattern formation.

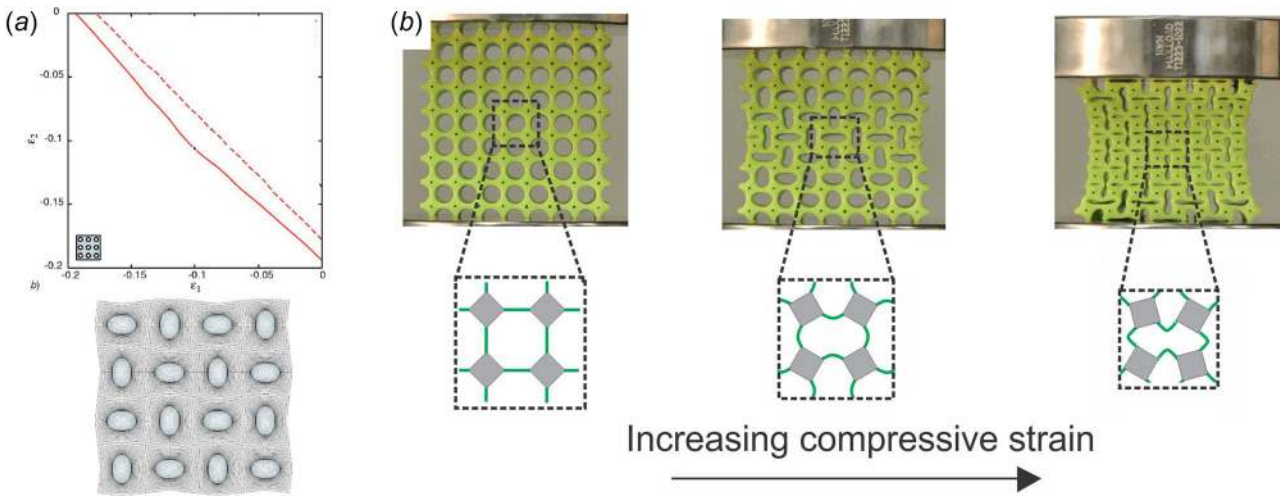

Fig. 10 (*a*) Macroscopic (continuous line) and microscopic (dashed line) onset-of-bifurcation surfaces in the principal macroscopic logarithmic strain space for a perfectly periodic neo-Hookean solid (characterized by a bulk to shear moduli ratio equal to 9.8) with a square distribution of circular voids. The eigenmode of the microscopic bifurcation instability is shown on the right. Reprinted with permission from Triantafyllidis et al. [162]. Copyright 2006 by ASME. (*b*) Experimental images of an elastomeric structure comprising a square array of circular holes for increasing values of the applied deformation. Note that after instability, the lateral boundaries of the sample bend inward, a clear signature of negative Poisson's ratio behavior. Adapted from Ref. [180].

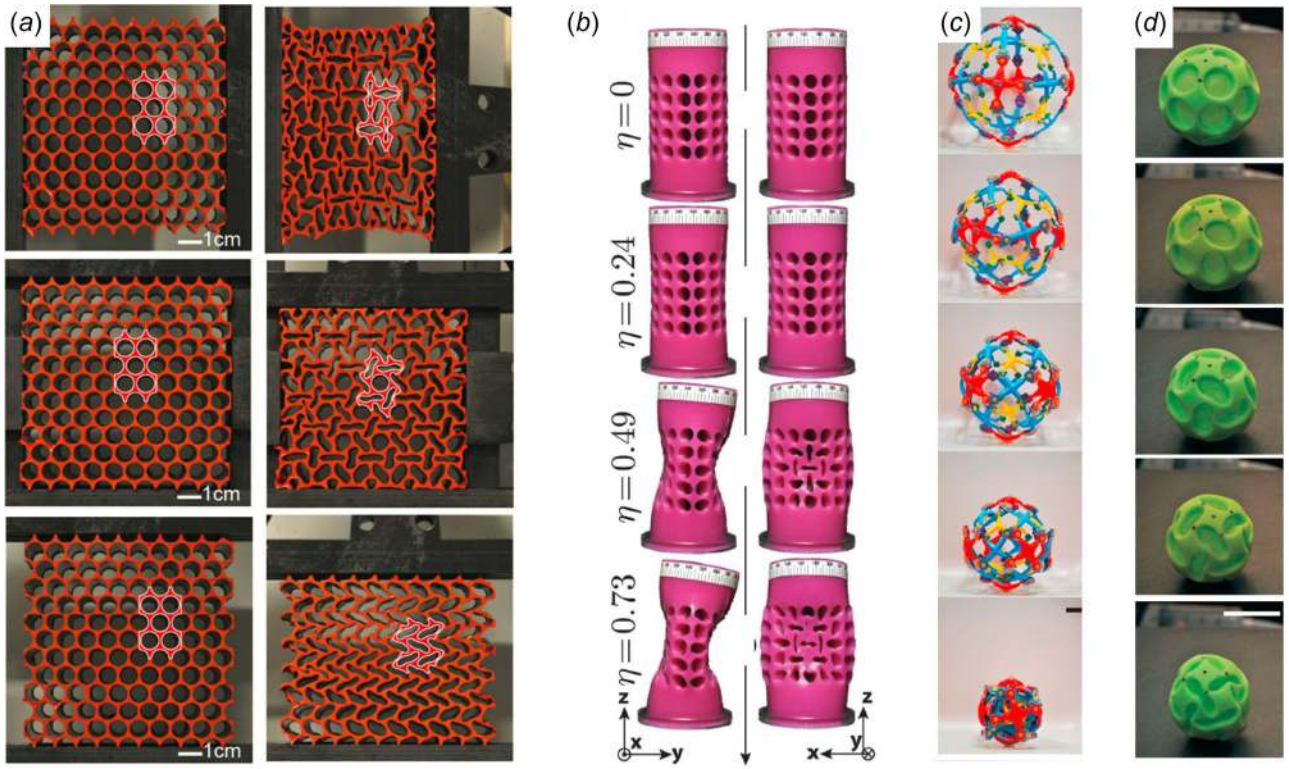

Fig. 11 (*a*) **Experimental images of an elastomeric structure comprising a triangular array of circular holes when compressed horizontally (top), vertically (center), and equibiaxially (bottom). Three distinct buckling-induced patterns are formed. Adapted from Ref. [174]. (*b*) Orthogonal side views (onto the *y–z* and *x–z* planes) for a cylindrical sample pattern with a square array of circular holes at different levels of deformation. The structure was made watertight by a thin membrane that covered the inner surface of the voids and was then loaded hydraulically. Adapted from Ref. [169]. (*c*) The Hoberman Twist-O is a commercial toy which comprises a rigid network of struts connected by rotating hinges and can easily collapse into a ball having a fraction of its original size. Adapted from Ref. [22]. (*d*) The Buckliball is inspired by this popular toy but translates the mechanism design to the structure of an elastic spherical shell—which under pneumatic actuation undergoes buckling-induced folding, opening avenues for a new class of active and reversible encapsulation systems. Adapted from Ref. [22].**

The pattern transformations triggered by instability in porous structures have been found to be robust and only marginally affected by small imperfections and edge effects [178]. However, their emergence can be compromised in structures characterized either by low levels of porosity or by multiple nucleation sites [163,166,185]. By progressively reducing the porosity, a transition

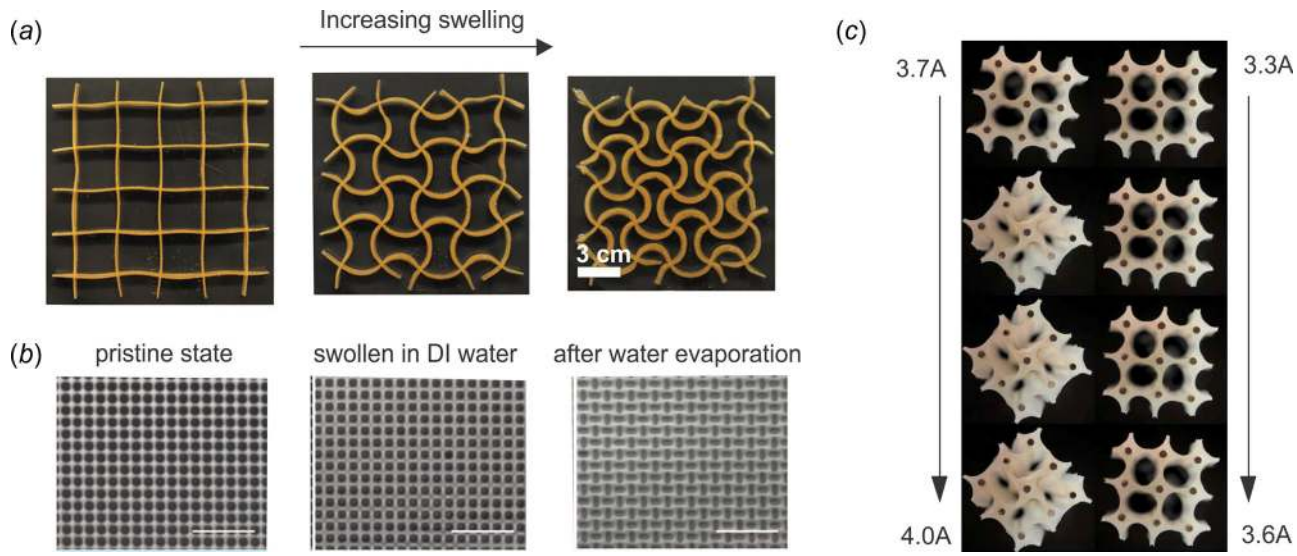

Fig. 12 (*a*) **Experimental snapshots during the swelling process for a square lattice made of plates sandwiched between two thin and stiff layers. Buckling induces an effective negative swelling ratio in this structure. Reprinted with permission from Liu et al. [165]. Copyright 2016 by John Wiley & Sons. (*b*) An instability is induced by capillary forces during evaporation of water from a swollen hydrogel membrane with micron-sized holes in a square array. Scale bars: 10 μm. Reprinted with permission from Zhu et al. [172]. Copyright 2012 by Royal Society of Chemistry (*c*) Slow variations in the current through several electromagnetic coils embedded in a soft cellular elastomer induce visible strain and snap-through behavior. Reprinted with permission from Tipton et al. [184]. Copyright 2012 by Royal Society of Chemistry.**

occurs from instabilities with a short wavelength to instabilities characterized by a wavelength much larger than the scale of the microstructure [163]. Differently, the presence of multiple nucleation sites results in domains of uniform buckling patterns separated by antiphase boundaries [166,185] (see Fig. 13(*a*)).

For elastic materials, these geometric reorganizations triggered by the instability are both reversible and repeatable. Furthermore, they occur over a narrow range of the applied load. Therefore, they do not only result in the formation of complex patterns but can also be instrumental to design materials with new modes of functionality. Recently, instabilities in periodic structures have been exploited to design metamaterials with tunable negative Poisson's ratio [163,164] (see Fig. 10) and effective negative swelling ratio [165] (see Fig. 12(*a*)), reversible encapsulation systems [22] (see Fig. 11(*d*)), structures capable of switching between achiral and chiral configurations [166–168] (see Fig. 13(*a*)), soft actuators [169] (see Fig. 11(*b*)) and robots [170] (see Fig. 13(*b*)), materials with tunable optical properties [171,172] (see Fig. 13(*c*)), and as described later, metamaterials with tunable dynamic response [34,173,174].

While most elastic instabilities are the result of compressive forces, elastic bodies may also become unstable under tensile loading. For example, a tension instability can be triggered in a block of incompressible elastic material under plane-strain conditions subjected to equibiaxial tension, resulting in its sudden flattening [186,187]. When a mechanical metamaterial is built by arranging such elastic blocks on a square lattice, an instability is triggered under equibiaxial tension resulting in a checkerboard pattern of pores with two different sizes [161,187,188]. Moreover, sequential snap-through instabilities triggered under tensile loading in mechanical metamaterials comprising 1D arrays of curved beams [189] (see Fig. 14(*a*)) and 2D arrays of rotating units [190] result in large extension and a range of nonlinear mechanical responses. Finally, mechanical instabilities in flat thin sheets with an embedded array of cuts subjected to uniaxial tension can result in out-of-plane deformation and the formation of 3D architectures [191,192] (see Fig. 14(*b*)), providing opportunities for the design of highly stretchable devices [193–198] and morphable structures [191,199,200].

It is also important to note that the formation of instability-driven patterns requires all building blocks to cooperatively deform (i.e., the metamaterial should be frustration-free). To achieve this, all slender elastic elements within the structure should buckle into the energetically most favored configuration and at the same time preserve the angles with their neighbors to minimize the deformation energy (see Fig. 15(*a*)). In two

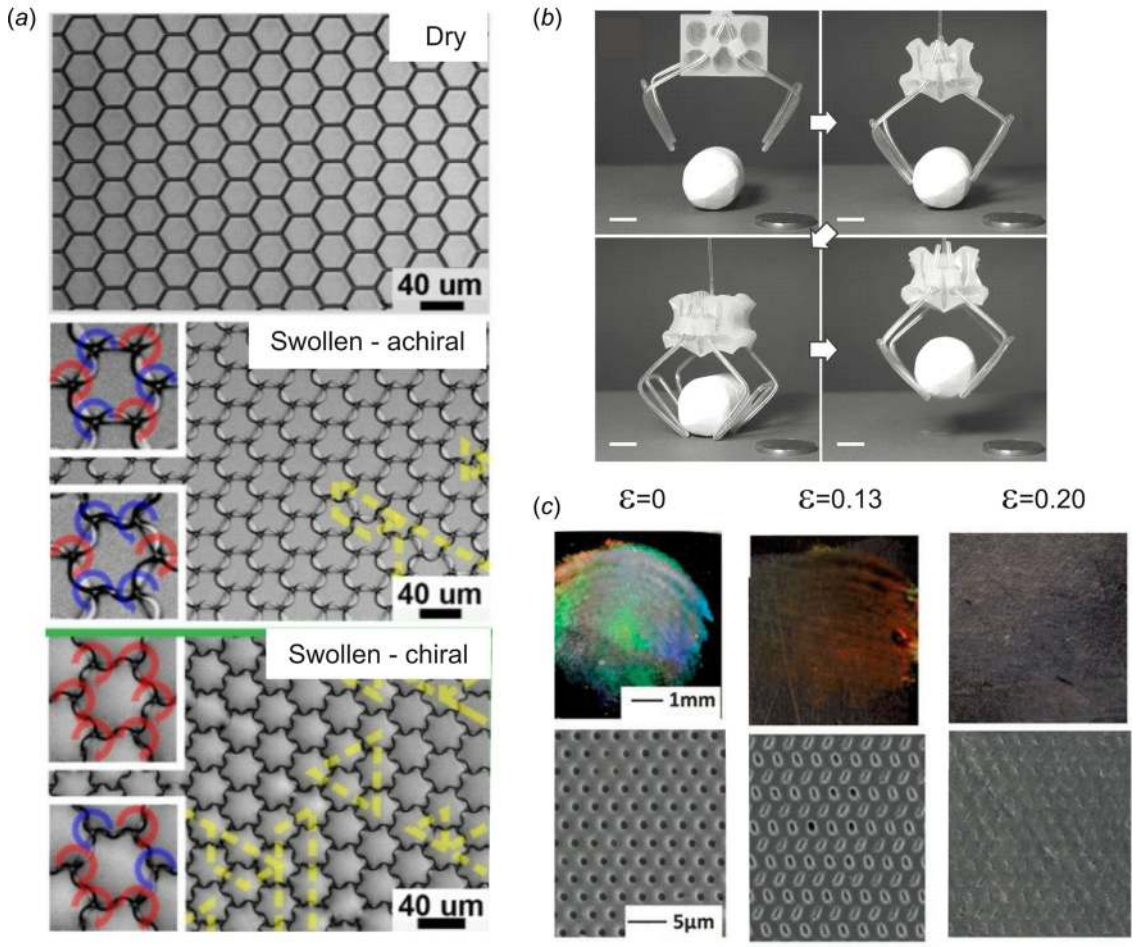

Fig. 13 (*a*) **Buckling-induced reversible pattern formation in a supported microscale honeycomb lattice upon rapid swelling. Depending on the geometry of the plates, buckling induces either an achiral pattern or a chiral pattern. Multiple domains with different chirality are observed, whose boundaries are highlighted by the dashed lines. The insets show magnified images of the buckled patterns within the domains (top) and at the domain boundaries (bottom). The color-coded arrows indicate the handedness of the vertices. Adapted from Ref. [166].** (*b*) **A soft gripper made of a buckling actuator. The claws of the gripper close upon deflation of the buckling actuator and the buckling gripper picks up a piece of chalk. Scale bars: 1 cm. Adapted from Ref. [170].** (*c*) **Buckling-induced pattern transformation in shape-memory polymer membranes comprising a hexagonal array of micron-sized circular holes results in dramatic color switching. Adapted from Ref. [171].**

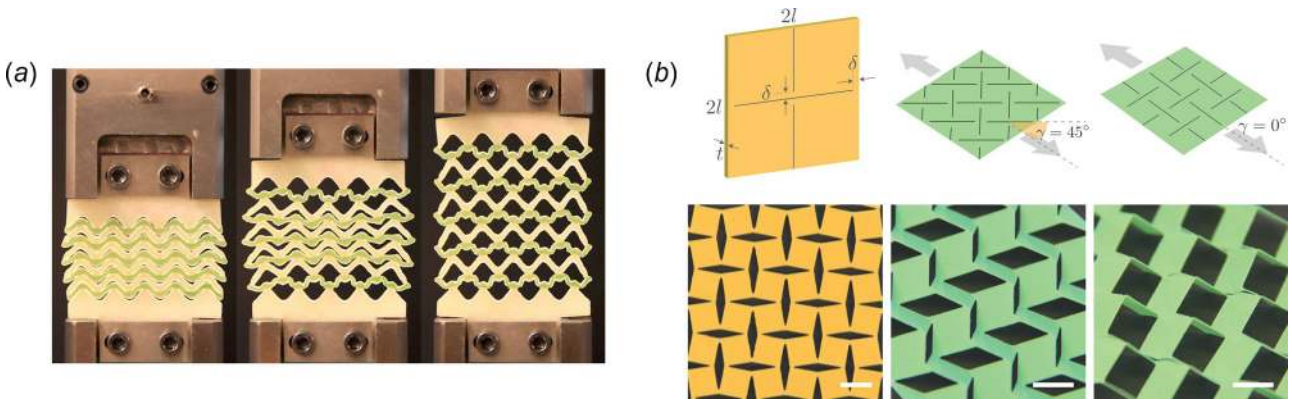

Fig. 14 (*a*) Snapshots of a bistable mechanical metamaterial in response to tensile loading. The system comprises an array of double-curved beams which can snap between two stable configurations. Adapted from Ref. [189]. (*b*) Response of an elastic sheet perforated with a square array of mutually orthogonal cuts under uniaxial tension. In the thick limit, the perforated sheet deforms in-plane and identically to a network of rotating squares (left). For sufficiently small values of thickness, mechanical instabilities triggered under uniaxial tension result in the formation of complex 3D patterns, which are affected by the loading direction (center and right). Scale bars: 6 mm. Adapted from Ref. [192].

dimensions, this rule can easily be satisfied on a square lattice, but not on a triangular one, so that the system becomes frustrated. While it has been shown that in periodic 2D beam lattices, geometric frustration favors the formation of complex ordered patterns [181] (see Fig. 15(*b*)), and in aperiodic architectures, it typically prevents a coherent and predictable response. However, a combinatorial strategy was introduced recently to design aperiodic and frustration-free mechanical metamaterials that exhibit spatially textured functionalities [201].

3.2.2 Tunable Acoustic Metamaterials. In recent years, rationally designed periodic structures have received increasing interest also because of their ability to manipulate and control the propagation of mechanical waves [202], opening avenues for a broad range of applications such as wave guiding [203,204], cloaking [205], noise reduction [206–208], and vibration control [209,210]. An important characteristic of these structured systems is their ability to tailor the propagation of waves due to the existence of band gaps—frequency ranges of strong wave attenuation—which can be generated either by Bragg scattering [211] or localized resonance within the medium [108].

While most of the proposed acoustic metamaterials operate in fixed ranges of frequencies that are impractical to tune and control after the assembly [212–217], it has been recently shown that instabilities provide an opportunity to alter in situ their dynamic response [34,35,173,218–221].

To study how instabilities and large deformations affect the propagation of small-amplitude elastic waves in periodic media, we consider an infinitesimal dynamic perturbation field **u** of the Bloch wave form (38) applied around an equilibrium state of final deformation φ^0. Insertion of Eq. (38) into Eq. (10) leads to the eigenvalue problem (41) to be solved on the periodicity of the irreducible Brillouin zone [222]. This eigenvalue problem is typically solved numerically using a number of techniques, including the plane-wave expansion method, the finite difference method, and the finite element method [202].

Equation (41) clearly indicates that the deformed solid or structure thus has a deformation-dependent (effective) incremental elasticity tensor $\mathbb{C}^0$ with generally anisotropic components. Therefore, predeformation allows for the controllable variation of elastic moduli and dispersion properties [221,223–225]. Such tunability can be further enhanced by triggering mechanical instabilities along the loading path, since these result in dramatic geometric reconfigurations.

Focusing on the structure presented in Fig. 10 (i.e., a square array of circular holes in an elastomeric matrix), it has been shown numerically that the pattern transformations occurring at instability strongly affect its Bragg-type band gaps [173,218]. More specifically, in the post-buckling regime some of the pre-existing band gaps close and new ones open (see Fig. 16), opening avenues for the design of acoustic switches to filter sound in a controlled manner. For weakly nonlinear materials (characterized by negligible stiffening effects induced by the applied deformation), the position and width of the band gaps are mainly determined by the geometric nonlinearities induced by the applied deformation, and the inhomogeneous stress state induced by the applied deformation has minimal effect. By contrast, for materials whose response is characterized by significant stiffening induced by the applied deformation, the material nonlinearity provides an additional tool to tune the position and width of the band gaps [218].

The topological changes induced by mechanical instabilities not only affect the band gaps but are also found to have a pronounced effect on the directionality of the propagating waves [218]. In the undeformed configuration (before buckling), an acoustic metamaterial comprising a square array of circular holes is anisotropic with larger wave speed along preferential directions [218]. More specifically, the phase velocity shows a preferred direction of propagation at $\theta = 45$ deg for mode 1 (shear-dominated mode) and at $\theta = 0$ deg for mode 2 (pressure-dominated mode) (see Fig. 17(*a*)). Moreover, the group velocity in the

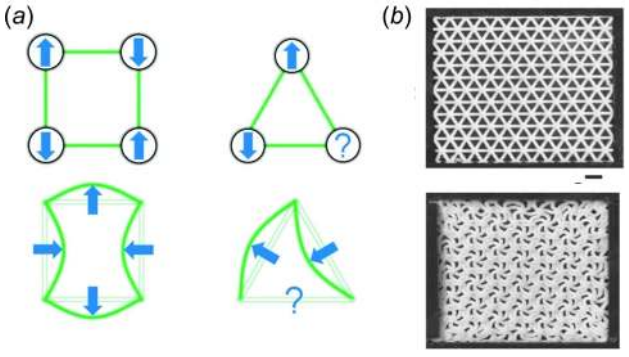

Fig. 15 (*a*) Analogously to antiferromagnetic systems—in which nearest-neighbor spins cannot align in opposite directions when arranged on a triangle—in triangular frames, the beams cannot buckle into a half sinusoid and at the same time preserve angles at joints. As a result, the system becomes frustrated. (*b*) Geometric frustration in periodic 2D beam lattices favors the formation of complex buckling-induced ordered patterns. Adapted from Ref. [181].

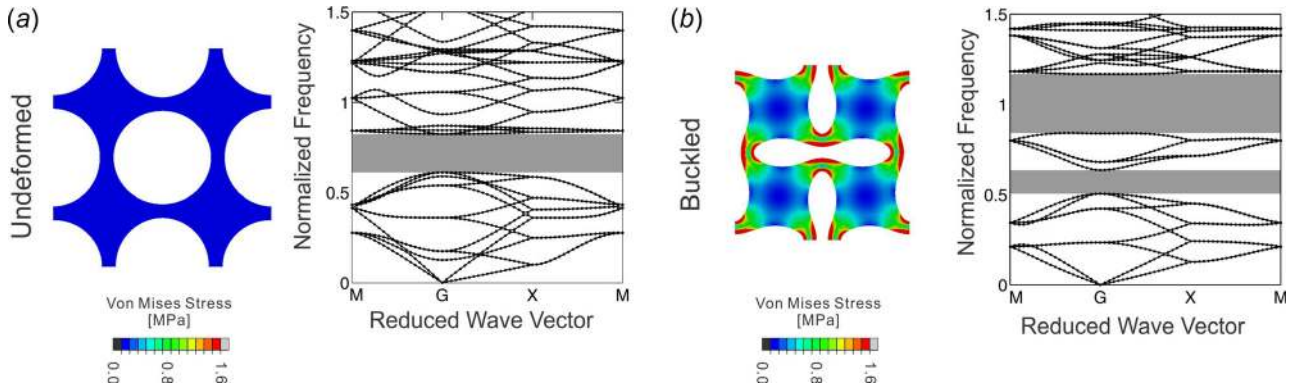

Fig. 16 Phononic band structure for a square array of circular voids in an elastic matrix subjected to equibiaxial compression in (*a*) the undeformed configuration and (*b*) after buckling. Adapted from Ref. [218].

undeformed configuration exhibits two preferred directions at $\theta = 10$ deg and 80 deg for mode 1 (see Fig. 17(*c*)), whereas it does not show a significant preferential direction of propagation for mode 2. In contrast, the buckled configuration does not exhibit any strong preference in directions for both phase and group velocities in both modes (see Figs. 17(*b*) and 17(*d*)), so that it behaves as a nearly isotropic medium. Finally, it has been shown that material nonlinearities do not affect the directionality of the propagating waves at low frequency and that only changes in geometry can be effectively used to tune the directional characteristics of the lower bands. This is due to the fact that the wavelengths of the low-frequency propagating modes are very long compared to the length scale of the local variations of the stress field.

Building on those results, tuning of Bragg-type band gaps has been demonstrated numerically for a number of systems, including hierarchical lattices [219], multilayers [35], and 3D architectures [220]. Moreover, enhanced tunability has been shown for acoustic metamaterials based on hexagonal honeycombs [174], since multiple and distinct buckling-induced patterns can be triggered by changing the loading direction [226–232].

Wave control through buckling is not limited to acoustic metamaterials with Bragg-type band gaps and can also be extended to systems with locally resonant band gaps. Experiments on acoustic metamaterials comprising resonating units consisting of a metallic core connected to the elastomeric matrix through elastic beams (see Fig. 18(*a*)) have shown that buckling can be intentionally exploited as an effective approach to control the propagation of elastic waves [34]. When the system is compressed statically, the beams connecting the resonators to the matrix buckle at a relatively low level of applied uniaxial (see Fig. 18(*b*)). Such buckling dramatically alters the stiffness of the beams and consequently the natural frequency of the resonating units, which in turn determines the frequency range of the band gap (see Fig. 18(*c*)). Interestingly, a moderate level of applied uniaxial strain ($\varepsilon \approx 0.10$) is found to

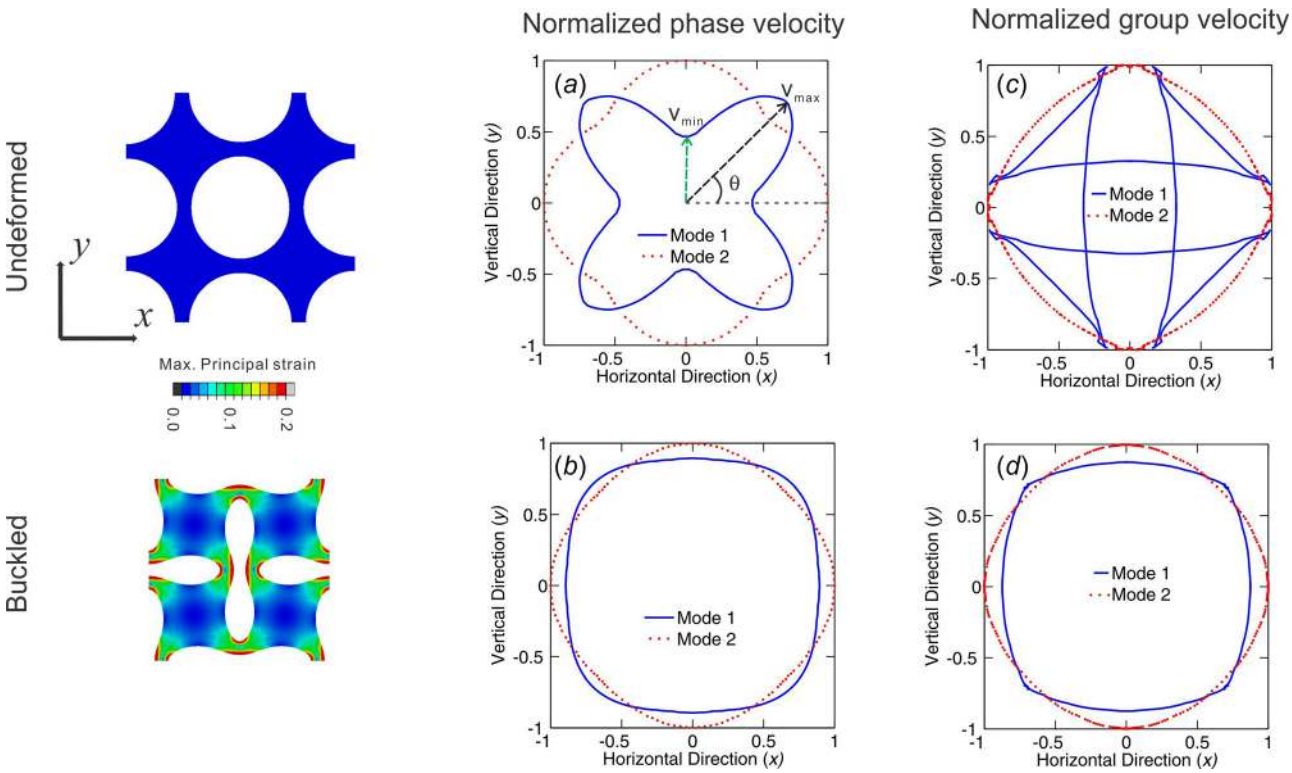

Fig. 17 Effect of deformation on the directionality of the propagating waves for a square array of circular voids in an elastic matrix subjected to equibiaxial compression. (*a*) and (*b*) Effect of deformation on the directionality of the phase velocity. (*c*) and (*d*) Effect of deformation on the directionality of the group velocity. Adapted from Ref. [218].

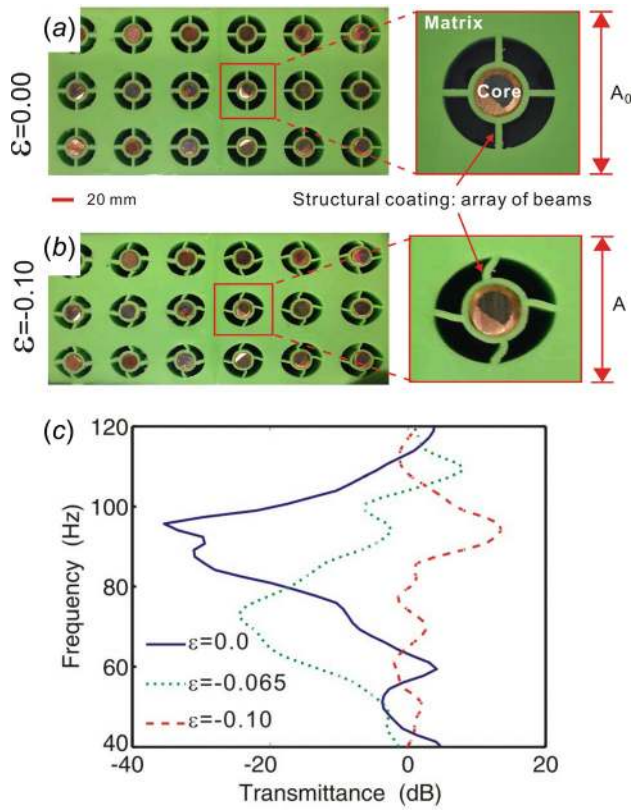

Fig. 18 Tunable acoustic metamaterial: (*a*) the undeformed configuration comprises resonating units dispersed into an elastomeric matrix. Each resonator consists of a metallic mass connected to the matrix through elastic beams, which form a structural coating. The black regions in the picture indicate voids in the structure. The unit cell size is $A_0 = 50.0$ mm. (*b*) When a compressive strain $\varepsilon = -0.10$ is applied in the vertical direction, buckling of the beams significantly alters the effective stiffness of the structural coating. (*c*) Experimentally measured transmittance at different levels of applied deformation. The band gap frequency first decreases linearly as a function of ε and then it completely disappears as ε approaches 0.10. Adapted from Ref. [34].

be enough to entirely suppress the band gap, so that the proposed metamaterial can be utilized as an on-or-off acoustic switch.

Finally, in addition to using instability to induce large deformations which in turn affect wave propagation, there has also been interest in acoustic metamaterials that exploit wave propagation through stabilized negative-stiffness components. For example, composites with negative-stiffness phases were shown to serve as waveguides with exceptional damping [129], and simple physical mass–spring models showed how the inclusion of negative-stiffness phases can lead to ultra-low resonant frequencies and tunable band gaps in the low-frequency regime [233].

3.2.3 Multistability and Nonlinear Metamaterials. Unlike most of the nonlinear elastic systems discussed earlier (which show patterns under applied loads or displacements), *multistable* systems possess two or more *stable* equilibrium states and can snap from one to another under applied external stimuli. The simple spring system of Fig. 2 is a classical example of a bistable structure with two stable equilibria, where the application of a load can drive the system from one equilibrium into the other (i.e., upon removal of the load, the system rests in the new equilibrium state). Multistability arises from a nonconvex, multiwelled potential energy landscape that results in inherently nonlinear behavior, see, e.g., Ref. [234]. Periodic arrays of multistable elementary unit cells produce interesting quasi-static patterns as in the soft hyperelastic metamaterials [174] discussed in Sec. 3.2.2. Those patterns can be tuned to either be space-filling, such as in most examples in Sec. 3.2.2 or in the 2D lattices made of bistable rods investigated in Ref. [235], or highly localized as in the selective buckling modes in the topological mechanical metamaterials of Ref. [236]. In the dynamic regime, multistability has been exploited in periodic metamaterials primarily in two ways.

First, the large mechanical hysteresis absorbs significant amounts of energy, so that multistable structures form exquisite building blocks for energy-absorbing media for applications such as impact mitigation and shock absorption. Examples range from the macroscale—where 3D-printed stacks of bistable beams absorb impact energy [237,238]—down to the nanoscale—where carbon nanotube buckling was explored to serve the same purpose [239]. In a similar spirit, multistable magnetoelastic structures (where multistability arises from the combination of magnetic and elastic interactions) were shown to efficiently absorb impact energy [240]. In all of these examples, the mechanical hysteresis associated with bi- or multistability absorbs large amounts of kinetic energy upon impact.

Second, periodic arrays of coupled multistable elements give rise to interesting dynamic phenomena involving large-amplitude nonlinear wave motion. As an introductory example, consider the spring–mass system of Fig. 2(*a*), which was shown to have the bistable energy landscape of Fig. 2(*c*). When the mass is excited dynamically, it may enter three regimes of motion: (i) infinitesimal excitations result in *linear elastic vibrations* of infinitesimal amplitude about one of the two equilibrium ground states, (ii) moderate-amplitude excitations lead to *weakly nonlinear* motion with fluctuations about one of the energy minima, and (iii) large excitations cause *strongly nonlinear* motion and snapping between the two equilibria. Under sustained forced loading, a large-amplitude oscillatory motion can be observed [241,242], which has been exploited, e.g., for energy harvesting [243,244] and vibration control [245]. For a thorough survey of the dynamic stability of elastic systems, see also Ref. [246].

Like in a metamaterial, let us periodically repeat the bistable unit cell of Fig. 2(*a*), which results in a chain of particles grounded nonlinearly and in a bistable onsite potential [247]. Again, small, moderate, and large excitations of the chain will result in, respectively, linear, weakly nonlinear, and strongly nonlinear wave motion [248]. To treat the problem more generally, consider an infinite 1D chain of particles at positions $\mathbf{x} = \{x_{-\infty}, \ldots, x_{\infty}\}$ with $x_j = ja$ and particle spacing a. Each particle has a mass m and is connected to its n neighbors on either side by an elastic potential V that depends on the strain $\varepsilon_{ij} = (x_j - x_i)/|j-i|a$ between two particles i and $j \neq i$. Assume that each particle is grounded in a nonlinear, multistable potential ψ (such as the bistable spring potential of Fig. 2(*c*)). The resulting total Hamiltonian $\mathcal{H}$ of the chain is

$$\mathcal{H}(\mathbf{x}, \dot{\mathbf{x}}) = \sum_{i=-\infty}^{\infty} \left[\frac{m}{2} |\dot{x}_i|^2 + \sum_{\substack{j=-n \\ j \neq 0}}^{n} V_j\left(\frac{x_{i+j} - x_i}{ja}\right) + \psi(x_i) \right] \tag{42}$$

The governing equations for all the particles follow from Hamilton's equations of motion. In the special case of linear springs of stiffness k connecting nearest-neighbor particles, we have $V_j(\varepsilon) = (k/2)(\varepsilon ja)^2$ and $n = 1$, and consequently

$$\mathcal{H}(\mathbf{x}, \dot{\mathbf{x}}) = \sum_{i=-\infty}^{\infty} \left[\frac{m}{2} |\dot{x}_i|^2 + \frac{k}{2}(x_{i+1} - x_i)^2 + \psi(x_i) \right] \tag{43}$$

Hamilton's equations yield the equation of motion for mass i in this case as

$$m\ddot{x}_i - k(x_{i+1} - 2x_i + x_{i-1}) + \frac{\partial \psi}{\partial x_i} = 0 \tag{44}$$

where the final term gives rise to nonlinearity.

A classic example of the previously mentioned form is the Frenkel–Kontorova model for dislocation motion in crystals [249,250] (based on an original model by Prandtl [251]). In this model, the periodic atomic lattice creates a multiwelled nonlinear potential with periodically repeating energy minima, which is approximated by the equation of motion

$$m\ddot{x}_i - k(x_{i+1} - 2x_i + x_{i-1}) + \sin\left(\frac{2\pi}{a}x_i\right) = 0 \tag{45}$$

We note that in case of smooth solutions with negligible discreteness or size effects [252], the continuum governing equations obtained from the limit $a \to 0$ may provide for closed-form solutions. For the Frenkel–Kontorova model, the continuum limit yields the Sine-Gordon equation [249,253]. An instructive experimental demonstration of the associated nonlinear wave motion was achieved in a 1D chain of rotating pendula coupled by elastic rotational springs [254].

As a further example of the same general structure, the Fermi–Pasta–Ulam model [255] describes, e.g., thermal equilibria of solids or hydrodynamic surface waves and is governed by

$$m\ddot{x}_i - k(x_{i+1} - 2x_i + x_{i-1}) + F(x_{i+1} - x_i) - F(x_i - x_{i-1}) = 0 \tag{46}$$

with nonlinear interaction forces $F(r)$. Its continuum limit is the Korteweg-de Vries equation [256,257].

Depending on the choice of the interaction potential and the multistable potential, such systems can propagate nonlinear signals, e.g., in the form of solitary waves. Under infinitesimal-amplitude loading, linear waves propagate in the classical acoustic sense. When excited by moderate and large amplitudes, the chain propagates weakly nonlinear solitons or strongly nonlinear transition waves [248].

Especially the propagation of transition waves has been of recent interest due to its potential for pulse propagation in lossy media. Consider the general form of the equation of motion obtained from Eq. (42) as

$$m\ddot{x}_i + \eta\dot{x}_i + \psi'(x_i) - \sum_{j=1}^{n}\left[V_j'\left(\frac{x_{i+j} - x_i}{ja}\right) - V_j'\left(\frac{x_i - x_{i-j}}{ja}\right)\right] = 0 \tag{47}$$

where we included a velocity-proportional damping term with viscosity $\eta > 0$ (every realistic system includes some level of energy dissipation).

As the multistable potential favors one of the multiple energy-minimizing equilibrium states while the interaction potential penalizes distance changes between particles, the chain under quasi-static conditions will form *domains* of equal particle equilibrium states separated by diffuse or sharp *domain walls* (across which the particles transition from one equilibrium to another), see Fig. 19. This phenomenon is well-known from materials that undergo, e.g., phase transformations [258], ferroelectric/magnetic domain switching [259–261], phase separation [262,263], or deformation twinning [51]. As shown in Fig. 15, similar domain patterns have also been observed in hyperelastic metamaterials when deformed nonlinearly to promote instabilities [181].

Under the action of loads or other external stimuli, domain walls move, which is a dissipative process that produces a macroscopically observable hysteresis and is of importance at the material level for, e.g., shape-memory alloys [264], ferroelectric poling [42], and multiferroics [265]. A moving domain wall is a transition wave (a topological soliton), which is propelled by the energy release of the snapping actions (each element switches from one stable equilibrium into another). In fact, it was shown that stable transition waves in a dissipative environment as described by Eq. (47) (in the continuum limit) obey the energy scaling law [266]

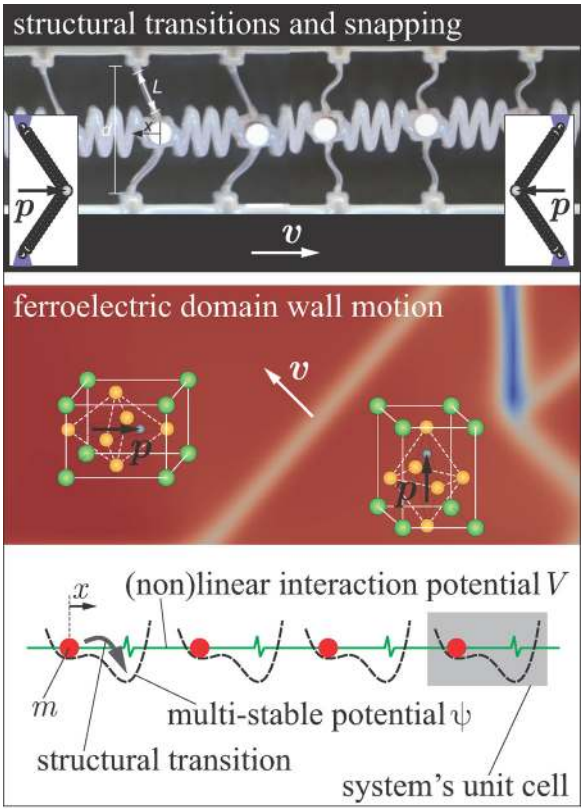

Fig. 19 Illustration of domains (constant polarization p within each domain) separated by domain walls in structures and materials. Under excitation, the domain walls move at speed *v*. The general structure of both systems is schematically shown with an interaction potential *V* and multistable potential ψ.

$$\frac{\Delta\psi}{2\gamma} = \frac{E}{v} \qquad \text{with} \qquad E = \int_{-\infty}^{\infty}\frac{1}{2}\dot{x}^2 ds \tag{48}$$

Here, $\Delta\psi = \psi^+ - \psi^-$ is the difference in the nonlinear energy potential before and after the transition wave, and v is the speed of the moving domain wall. γ is the continuum damping density (related to η, see Ref. [266] for details) and $x(s, t)$ is the continuum limit of the discrete particle positions in the chain described by a spatial coordinate s. E represents the kinetic energy per mass density of the moving domain wall. Since $E \geq 0$ by definition and $\gamma \geq 0$ by the second law of thermodynamics, we must have $\Delta\psi \cdot v > 0$ for a transition wave to exist. In other words, in the presence of damping, a domain wall will only move in a direction that jumps from a high-energy equilibrium to a low-energy equilibrium. This is of interest for the support of unidirectional wave propagation such as in mechanical diodes [23,267].

Moreover, for linear damping, the amount of energy released by snapping from the high-energy to the low-energy state is dissipated, which leads to a transition wave moving at constant speed [266]. This is quite remarkable as it predicts the propagation of a nonlinear, large-amplitude wave of constant speed over, in principle, infinite distances in a lossy medium. This concept was recently demonstrated experimentally in two distinct settings. First, experiments in Ref. [267] realized transition waves in a chain of bistable, buckled composite shells (creating a bistable, asymmetric potential ψ) which were coupled by repelling permanent magnets (producing a nonlinear interaction potential V with practically beyond-nearest-neighbor interactions), see Fig. 20. Second, experiments in Ref. [23] used 3D-printing to produce long chains of linear elastically coupled, buckled, bistable beams, see Fig. 21. In both cases, experiments indeed revealed stable transition waves of constant speed over long distances (see, e.g.,

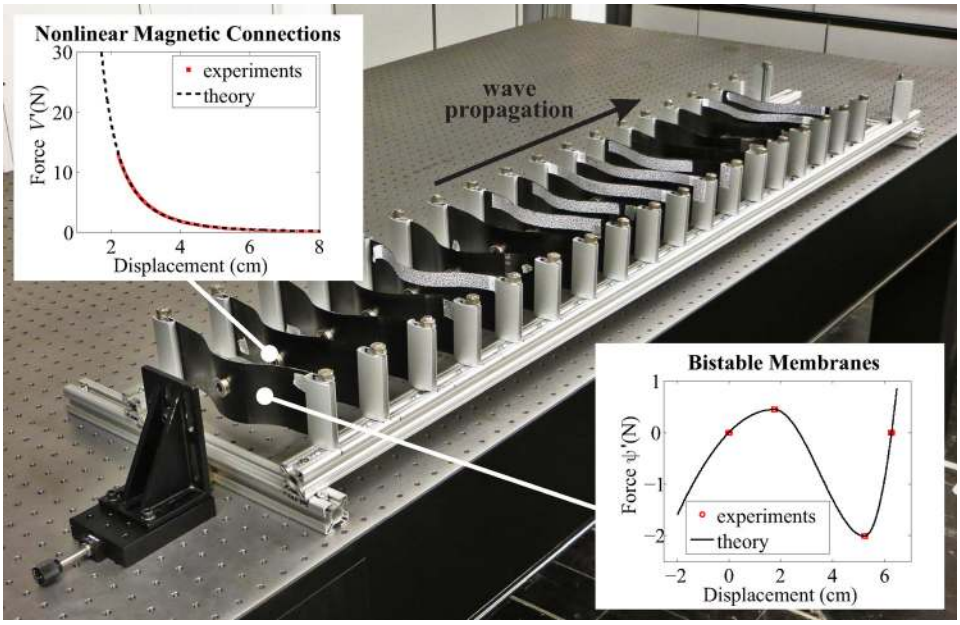

Fig. 20 A chain of laterally compressed, bistable membranes coupled by nonlinear permanent magnets obeys Eq. (47) and displays unidirectional transition wave motion upon impact [266]

the measured x–t-diagram of the moving transition wave in Fig. 21(*b*), having a constant slope and thus constant speed after a brief initial transient phase). Especially, the 3D-printed setup made of lossy polymeric base materials displayed significant damping which quickly attenuated all linear waves but allowed the propagation of the constant-speed transition wave.

These structural 1D examples do not only qualitatively resemble domain wall motion in materials (as schematically shown in Fig. 19). Phase transitions or ferroelectric switching are commonly modeled by phase field models. The time evolution in those models is usually derived from the assumption of gradient flow, resulting in the Allen–Cahn equation [268]

$$\eta\,\dot{\chi} = -\frac{\delta W}{\delta \chi} = -\psi'(\chi) + \kappa\,\nabla^2\chi \tag{49}$$

where χ denotes a polarization field (or phase field parameter), W is the energy density, and its variational derivative involves a nonlinear term (stemming from the multistable potential ψ) and a nonlocal term accounting for interfacial energy in this diffuse-interface setting. For example, in ferroelectrics $\chi = \mathbf{p}$ denotes the ferroelectric polarization vector [260,261,269] and ψ is a multiwelled potential having $2d$ symmetric minima in d dimensions (whose symmetry is broken by an applied electric field). Notice that, with $V = (\kappa/2)||\nabla\chi||^2$, Eq. (49) has the same structure as the continuum limit of Eq. (47) except that $m = 0$. As the scaling law (48) is independent of the mass (or mass density) of the chain, it still applies. Therefore, Eq. (49) obeys quantitatively the same scaling laws as Eq. (47).

Similar nonlinear kinetics showing the general structure of Eq. (47) can be found in models for dislocation motion [249], ferromagnetic domain wall motion [270], proton mobility in hydrogen-bonded chains [271], rotation of DNA bases [272], chains of rotating pendula [254], dynamics of carbon nanotube foams [239,273], magnetic flux propagation in Josephson junctions [274], pulse propagation in cardiophysiology [275] and neurophysiology [276], or chemical surface adsorption [277]. Over decades, those have motivated numerous theoretical studies to characterize the motion of domain walls and phase boundaries particularly in 1D periodic physical, chemical, or biological systems, see, e.g., Refs. [117] and [278–285]. A related phenomenon is the transition wave-like propagation of signals in chains made of rigid elements with zero-energy modes [286]. Here, mechanisms result in edge modes that can propagate along the chain.

At the structural level, those concepts have been extended to higher dimensions, which have resulted in metamaterials or

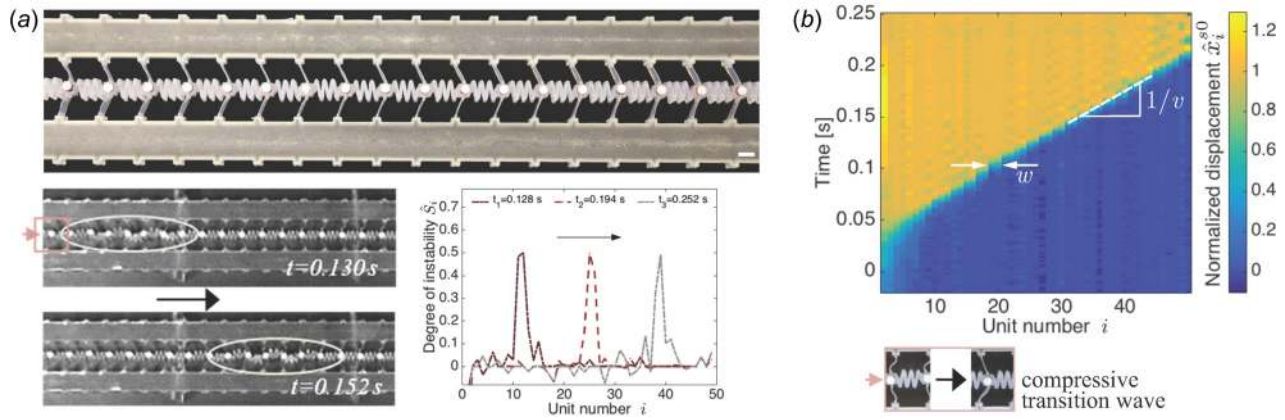

Fig. 21 Stable transition waves in a 3D-printed chain of bistable elements [23]: (*a*) a compressive transition wave propagates by releasing stored elastic energy, which is dissipated due to material-internal damping mechanisms. (*b*) A stable transition wave of constant speed *v* and width *w* is recorded (after an initial transient period).

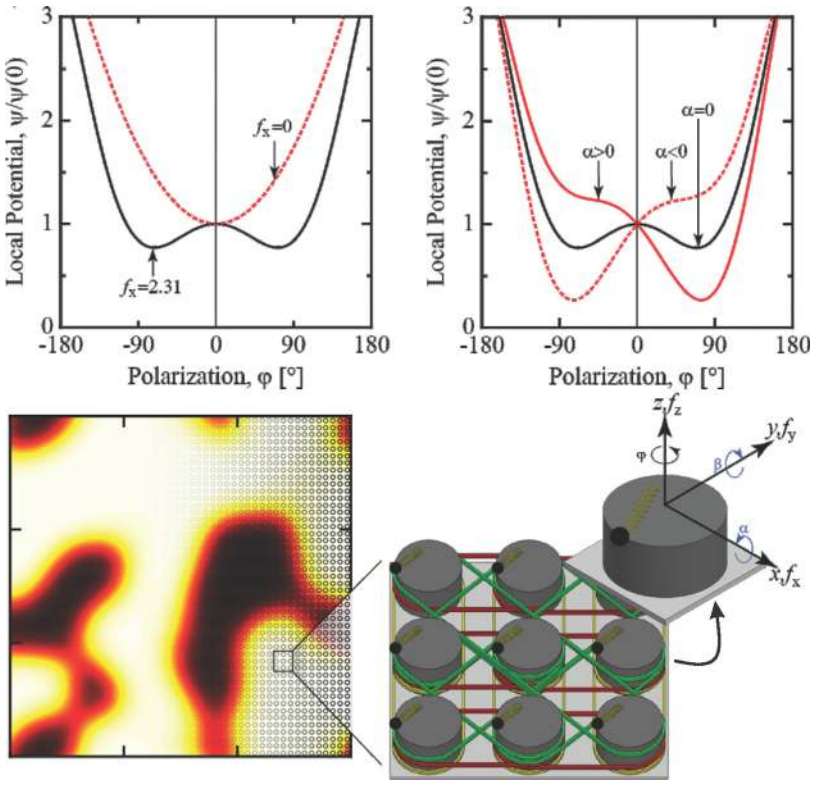

Fig. 22 Periodic array of bistable rotational elements (polarization angle φ) coupled to nearest neighbors by elastic bands [287]. The combination of an excentrically attached linear spring and the action of gravity results in a tunable bistable potential ψ which can be biased as in domain switching (by tilting the whole setup by an angle α) and which can also mimic a second-order phase transition (by adjusting the position f_x of the spring anchor points, switching between a bistable potential and a single-well potential).

structures displaying complex domain walls. Recently, the concept was extended to promote nonlinear dynamic domain evolution in 2D structures or metamaterials. Guided by the same principles and governing equations discussed earlier for 1D chains, the setup of Fig. 22 is made of rotational masses and linear spring connections. In addition to linear elastic bands connecting the rotational masses (producing interaction potential V), eccentrically attached elastic springs and gravity are exploited to produce a bistable onsite potential ψ for each mass, favoring one of two symmetric equilibrium angles (the rotational angle φ serves as the "polarization" field here). Under the action of gravitational forces, tilting of the whole system mimics the application of an electric field in that it favors one of the two stable equilibria. This setup was shown to follow the same governing equations discussed earlier, and it reproduced typical behavior found in materials during domain switching as well as during second-order phase transformations [287].

4 Discussion

Exploiting instability in solids and structures has offered new opportunities and opened new directions in mechanics research. The broad range of materials and applications taking advantage of instability extends from buckling and swelling in soft elastomeric structures to topological transformations in structures, solids, and metamaterials in between those. Properties of interest include the quasi-static behavior (such as stiffness, strength, and energy absorption) as well as the dynamic response (such as in photonic, phononic, acoustic, or nonlinear wave guides and metamaterials). Although exciting research has been reported in all those directions, as described in this review, a number of open challenges have remained, summarized in this nonexhaustive list:

- Research has focused primarily on either the linear—static and dynamic—response of structures and solids (targeting, e.g., the effective stiffness or wave dispersion) or on their nonlinear quasi-static behavior (e.g., maximizing strength or inducing large configurational changes through finite-deformation instabilities in soft matter). Nonlinearity and dynamics have most commonly been combined in the form of large quasi-static preloads, upon which linear waves are superimposed. *Nonlinear dynamic* effects are much richer but also much more complex and have been investigated only recently, as described in Sec. 3.2.3, and leave room for further investigation.
- Most research on stability-induced acoustic waveguides, as described in Sec. 3.2.2, has employed methods of additive manufacturing, specifically 3D printing of polymeric structures. Those come with *high internal friction* which prevents effective wave propagation over long distances. Realizing comparable well-controlled instabilities in stiff structures (which would allow for stable wave propagation with low losses) is a challenge and has been limited to, primarily, impact mitigation. Stiff bistable structures have been made, e.g., out of bulk metallic glass [288]. Key is to design slender structures that accommodate large deformations with small strains. However, this considerably restricts the design space. Recoverability is another concern in stiff systems, which may hint at advantages at very small scales where size effects alter the recoverability of, e.g., hollow nanolattices [25].
- Structural instabilities are scale-independent (and may enter only through size effects that affect the base material properties). For simplicity, metamaterials exploiting instability are typically investigated at the macroscopic centimeter-scale (see Sec. 3.2), whereas most applications require *miniaturization*

down to smaller scales with unit cell sizes on the order of microns and below. This calls for improved, *scalable fabrication tools* to produce computationally optimized metamaterial designs at relevant scales. Of course, this also comes with the need for *high-precision experimental techniques* at small scales to verify the performance.

- With decreasing size, one ultimately reaches scales at which *fluctuations* matter significantly more than at the macroscopic scale. Imperfections affect the performance of structures and metamaterials at all scales (such as geometric or local material imperfections), especially when it comes to instabilities. However, imperfections tend to play greater roles with decreasing size. For example, fabrication-induced *imperfections* in 3D-printed structures are small compared to feature sizes at the centimeter-scale, whereas the printing of structures and metamaterials at the micron-scale necessarily produces imperfections that are—relatively—considerably larger compared to feature sizes. This calls for, again, new high-precision fabrication techniques but also for theoretical-computational tools to reliably predict the performance of metamaterials with realistic imperfections. Another type of fluctuations, *thermal effects* in nano- to micron-scale systems generally affect all kinetic processes but especially those associated with instabilities, owing to their high sensitivity to small perturbations [289]. Such thermalization has no macroscopic analog, which results in an interesting breakdown of micro–macro analogies between materials and metamaterials.
- Most of the examples reviewed earlier have focused on instabilities and multistability arising in mechanical systems. By contrast, *multiphysics* systems such as magnetomechanically, electromechanically, or electromagnetomechanically coupled materials as well as chemomechanically coupled solids offer a myriad of opportunities for coupled phenomena—both in the quasi-static response as well as in terms of coupled wave propagation and nonlinear dynamic behavior. Only few examples exist where metamaterials deliberately exploit the multiphysics setting to create multistability, see, e.g., Ref. [240]. In addition, the response of materials to external stimuli such as electric, magnetic, or thermal fields, chemical or biological agents, or physical stimuli such as light offers opportunities that have not been fully explored in the context of instability.
- The *negative-stiffness concept* is one of the few examples where multiphysics in the form of (thermoelectromechanically coupled) phase transformations have played a central role (see Sec. 3.1). To date, only a few representative examples of composite materials realizing this phenomenon have been reported (see Sec. 3.1.4). In addition, the reported strong variations in stiffness and damping in response to temperature changes are hard to control, which is why replacing temperature control by, e.g., electric or magnetic fields would be a welcome alternative but has not yet resulted in viable applications of actively tunable materials systems. Negative stiffness in structures was primarily exploited for vibration attenuation in macroscopic devices. Metamaterials that stabilize small-scale structural instabilities to create positive- and negative-stiffness composite systems have remained a rare find.
- The metamaterials community has targeted a number of interesting material properties and material property combinations (some of which have been discussed earlier). Classics are stiffness, strength, damping, energy absorption, linear wave dispersion, and refraction, and more recently nonlinear waves. In many of those examples, inspiration was drawn from structure–property relations in materials, whose mimicking at the structural scale resulted in metamaterials with controllable properties. There are probably many further material properties or performance metrics that allow for a similar micro-to-macro correspondence and that may benefit from exploiting instabilities. Fracture toughness is an example that may involve path-dependent material behavior and is harder to control than the classical, linear properties of interest. Instability has played a role both at the structural scale (e.g., by exploiting "waiting links" and delocalizing damage [117,290]) and at the material level (e.g., by exploiting phase transformations ahead of the crack tip to effect transformation toughening [291]).

5 Conclusions

We have reviewed the state-of-the-art in utilizing instabilities in solids and structures to achieve beneficial effective performance. To this end, we first reviewed the fundamental principles of stability theory, followed by examples of exploiting instability in both materials (e.g., through the negative-stiffness concept) and in structures and metamaterials (e.g., through instability-inducing large shape changes that allow the control of the effective properties). We believe that this is a still young area which—despite the tremendous recent progress surveyed in this contribution—has still left many open questions and opportunities for future research.

Funding Data

- National Science Foundation, Division of Civil, Mechanical and Manufacturing Innovation (CAREER Award Nos. CMMI-1254424 and CMMI-1149456).
- Division of Materials Research (Grant No. DMR-1420570).
- Office of Naval Research (Grant No. W911NF-17-1-0147).

References

[1] Euler, L., 1759, "Sur la force des colonnes," Mem. Acad. Berlin, **13**, pp. 252–282.
[2] Euler, L., 1778, "De altitudine colomnarum sub proprio pondere corruentium," Acta Acad. Sci. Petropolitana, **1**, pp. 191–193.
[3] Euler, L., 1780, "Determinatio onerum quae columnae gestare valent," Acta Acad. Sci. Petropolitana, **2**, pp. 163–193.
[4] Kirchhoff, G., 1859, "Über das Gleichgewicht und die Bewegung eines unendlich dünnen elastischen Stabes," J. Reine Angew. Math., **1859**(56), pp. 285–313.
[5] Love, A., 1893, *Mathematical Theory of Elasticity*, Cambridge Press, Cambridge, MA.
[6] Thomson, W. L. K., 1875, "Elasticity," *Encyclopedia Britannica*, Vol. 7, Encyclopædia Britannica, Inc., London.
[7] Lord Rayleigh, F. R. S., 1878, "On the Instability of Jets," Proc. London Math. Soc., **s1-10**(1), pp. 4–13.
[8] Southwell, R. V., 1914, "On the General Theory of Elastic Stability," Philos. Trans. R. Soc. London A, **213**(497–508), pp. 187–244.
[9] Timoshenko, S., and Gere, J., 1961, *Theory of Elastic Stability*, McGraw-Hill, New York.
[10] Leipholz, H., 1970, *Stability Theory*, Academic Press, New York.
[11] Thompson, J., and Hunt, G., 1973, *A General Theory of Elastic Stability*, Wiley, New York.
[12] Iooss, G., and Joseph, D., 1980, *Elementary Bifurcation and Stability Theory*, Springer, New York.
[13] Geymonat, G., Müller, S., and Triantafyllidis, N., 1993, "Homogenization of Nonlinearly Elastic Materials, Microscopic Bifurcation and Macroscopic Loss of Rank-One Convexity," Arch. Ration. Mech. Anal., **122**(3), pp. 231–290.
[14] Como, M., and Grimaldi, A., 1995, *Theory of Stability of Continuous Elastic Structures*, CRC Press, Boca Raton, FL.
[15] Nguyen, Q., 2000, *Stability and Nonlinear Solid Mechanics*, Wiley, New York.
[16] Ziegler, H., 1968, *Principles of Structural Stability*, Blaisdell, New York.
[17] Simitses, G. J., and Hodges, D. H., 2006, *Fundamentals of Structural Stability*, Butterworth-Heinemann, Burlington, MA.
[18] Knops, R., and Wilkes, W., 1973, "Theory of Elastic Stability," *Handbook of Physics*, Vol. VIa, Springer, Berlin, p. 125302.
[19] Budiansky, B., 1974, "Theory of Buckling and Post-Buckling Behavior in Elastic Structures," *Advances of Applied Mechanics*, Elsevier, Amsterdam, The Netherlands, pp. 1–65.
[20] Goncu, F., Willshaw, S., Shim, J., Cusack, J., Luding, S., Mullin, T., and Bertoldi, K., 2011, "Deformation Induced Pattern Transformation in a Soft Granular Crystal," Soft Matter, **7**(6), pp. 2321–2324.
[21] Overvelde, J., Shan, S., and Bertoldi, K., 2012, "Compaction Through Buckling in 2D Periodic, Soft and Porous Structures: Effect of Pore Shape," Adv. Mater., **24**(17), pp. 2337–2342.

[22] Shim, J., Perdigou, C., Chen, E., Bertoldi, K., and Reis, P., 2012, "Buckling-Induced Encapsulation of Structured Elastic Shells Under Pressure," Proc. Natl. Acad. Sci., **109**(16), pp. 5978–5983.
[23] Raney, J. R., Nadkarni, N., Daraio, C., Kochmann, D. M., Lewis, J. A., and Bertoldi, K., 2016, "Stable Propagation of Mechanical Signals in Soft Media Using Stored Elastic Energy," Proc. Natl. Acad. Sci., **113**(35), pp. 9722–9727.
[24] Tavakol, B., Bozlar, M., Punckt, C., Froehlicher, G., Stone, H. A., Aksay, I. A., and Holmes, D. P., 2014, "Buckling of Dielectric Elastomeric Plates for Soft, Electrically Active Microfluidic Pumps," Soft Matter, **10**(27), pp. 4789–4794.
[25] Meza, L. R., Das, S., and Greer, J. R., 2014, "Strong, Lightweight, and Recoverable Three-Dimensional Ceramic Nanolattices," Science, **345**(6202), pp. 1322–1326.
[26] Meza, L. R., Zelhofer, A. J., Clarke, N., Mateos, A. J., Kochmann, D. M., and Greer, J. R., 2015, "Resilient 3D Hierarchical Architected Metamaterials," Proc. Natl. Acad. Sci., **112**(37), pp. 11502–11507.
[27] Lee, J.-H., Ro, H. W., Huang, R., Lemaillet, P., Germer, T. A., Soles, C. L., and Stafford, C. M., 2012, "Anisotropic, Hierarchical Surface Patterns Via Surface Wrinkling of Nanopatterned Polymer Films," Nano Lett. **12**(11), pp. 5995–5999.
[28] Pezzulla, M., Shillig, S. A., Nardinocchi, P., and Holmes, D. P., 2015, "Morphing of Geometric Composites Via Residual Swelling," Soft Matter, **11**(29), pp. 5812–5820.
[29] Platus, D. L., 1999, "Negative-Stiffness-Mechanism Vibration Isolation Systems," Proc. SPIE, **3786**, pp. 98–105.
[30] Yap, H. W., Lakes, R. S., and Carpick, R. W., 2008, "Negative Stiffness and Enhanced Damping of Individual Multiwalled Carbon Nanotubes," Phys. Rev. B, **77**(4), p. 045423.
[31] Mizuno, T., 2010, "Vibration Isolation System Using Negative Stiffness," *Vibration Control*, Vol. 3786, M. Lallart, ed., InTech, Rijeka, Croatia.
[32] Lee, C.-M., and Goverdovskiy, V., 2012, "A Multi-Stage High-Speed Railroad Vibration Isolation System With Negative Stiffness," J. Sound Vib., **331**(4), pp. 914–921.
[33] Goncu, F., Luding, S., and Bertoldi, K., 2012, "Exploiting Pattern Transformation to Tune Phononic Band Gaps in a Two-Dimensional Granular Crystal," J. Acoust. Soc. Am., **131**(6), pp. EL475–EL480.
[34] Wang, P., Casadei, F., Shan, S., Weaver, J., and Bertoldi, K., 2014, "Harnessing Buckling to Design Tunable Locally Resonant Acoustic Metamaterials," Phys. Rev. Lett., **113**, p. 014301.
[35] Rudykh, S., and Boyce, M., 2014, "Transforming Wave Propagation in Layered Media Via Instability-Induced Wrinkling Interfacial Layer," Phys. Rev. Lett., **112**(3), p. 034301.
[36] Xin, F., and Lu, T., 2016, "Tensional Acoustomechanical Soft Metamaterials," Sci. Rep., **6**, p. 27432.
[37] Lakes, R. S., 2001, "Extreme Damping in Compliant Composites With a Negative-Stiffness Phase," Philos. Mag. Lett., **81**(2), pp. 95–100.
[38] Lakes, R. S., 2001, "Extreme Damping in Composite Materials With a Negative Stiffness Phase," Phys. Rev. Lett., **86**(13), pp. 2897–2900.
[39] Lakes, R. S., Lee, T., Bersie, A., and Wang, Y. C., 2001, "Extreme Damping in Composite Materials With Negative-Stiffness Inclusions," Nature, **410**(6828), pp. 565–567.
[40] Jaglinski, T., Kochmann, D., Stone, D., and Lakes, R. S., 2007, "Composite Materials With Viscoelastic Stiffness Greater Than Diamond," Science, **315**(5812), pp. 620–622.
[41] Popa, B.-I., Zigoneanu, L., and Cummer, S. A., 2013, "Tunable Active Acoustic Metamaterials," Phys. Rev. B, **88**(2), p. 024303.
[42] Wojnar, C. S., le Graverend, J.-B., and Kochmann, D. M., 2014, "Broadband Control of the Viscoelasticity of Ferroelectrics Via Domain Switching," Appl. Phys. Lett., **105**(16), p. 162912.
[43] Reis, P. M., 2015, "A Perspective on the Revival of Structural (In)Stability With Novel Opportunities for Function: From Buckliphobia to Buckliphilia," ASME J. Appl. Mech., **82**(11), p. 111001.
[44] Morrey, C. B., 1952, "Quasi-Convexity and the Lower Semicontinuity of Multiple Integrals," Pac. J. Math., **2**(1), p. 25–53.
[45] Knops, R. J., and Stuart, C. A., 1986, *Quasiconvexity and Uniqueness of Equilibrium Solutions in Nonlinear Elasticity*, Springer, Berlin, pp. 473–489.
[46] Landau, L., 1937, "On the Theory of Phase Transitions," Zh. Eksp. Teor. Fiz., **7**, pp. 19–32 (in Russian).
[47] Devonshire, A., 1949, "XCVI. Theory of Barium Titanate," Philos. Mag., **40**(309), pp. 1040–1063.
[48] Devonshire, A., 1951, "CIX. Theory of Barium Titanate: Part II," Philos. Mag., **42**(333), pp. 1065–1079.
[49] Ball, J., and James, R., 1987, "Fine Phase Mixtures as Minimizers of Energy," Arch. Ration. Mech. Anal., **100**(1), pp. 13–52.
[50] James, R., 1981, "Finite Deformation by Mechanical Twinning," Arch. Ration. Mech. Anal., **77**(2), pp. 143–176.
[51] Christian, J., and Mahajan, S., 1995, "Deformation Twinning," Prog. Mater. Sci., **39**(1–2), pp. 1–157.
[52] Carstensen, C., Hackl, K., and Mielke, A., 2002, "Non-Convex Potentials and Microstructures in Finite-Strain Plasticity," Proc. R. Soc. London, Ser. A, **458**(2018), pp. 299–317.
[53] Ortiz, M., and Repettto, E. A., 1999, "Nonconvex Energy Minimization and Dislocation Structures in Ductile Single Crystals," J. Mech. Phys. Solids, **47**(2), pp. 397–462.
[54] Govindjee, S., Mielke, A., and Hall, G. J., 2003, "The Free Energy of Mixing for n-Variant Martensitic Phase Transformations Using Quasi-Convex Analysis," J. Mech. Phys. Solids, **51**(4), pp. I–XXVI.
[55] Miehe, C., Lambrecht, M., and Gurses, E., 2004, "Analysis of Material Instabilities in Inelastic Solids by Incremental Energy Minimization and Relaxation Methods: Evolving Deformation Microstructures in Finite Plasticity," J. Mech. Phys. Solids, **52**(12), pp. 2725–2769.
[56] Bhattacharya, K., 2004, *Microstructure of Martensite—Why It Forms and How It Gives Rise to the Shape-Memory Effect*, Oxford University Press, Oxford, UK.
[57] Lee, J.-H., Singer, J. P., and Thomas, E. L., 2012, "Micro/Nanostructured Mechanical Metamaterials," Adv. Mater., **24**(36), pp. 4782–4810.
[58] Spadaccini, C. M., 2015, "Mechanical Metamaterials: Design, Fabrication, and Performance," Winter, **45**(4), pp. 28–36.
[59] Li, X., and Gao, H., 2016, "Mechanical Metamaterials: Smaller and Stronger," Nat. Mater., **15**, pp. 373–374.
[60] Papanicolaou, G., Bensoussan, A., and Lions, J., 1978, *Asymptotic Analysis for Periodic Structures. Studies in Mathematics and Its Applications*, North-Holland, Amsterdam, The Netherlands.
[61] Sánchez-Palencia, E., 1980, *Non-Homogeneous Media and Vibration Theory* (Lecture Notes in Physics), Springer, New York.
[62] Schröder, J., 2000, "Homogenisierungsmethoden der nichtlinearen kontinuumsmechanik unter beachtung von stabilitätsproblemen," Ph.D. thesis, Universität Stuttgart, Stuttgart, Germany.
[63] Terada, K., and Kikuchi, N., 2001, "A Class of General Algorithms for Multi-Scale Analyses of Heterogeneous Media," Comput. Methods Appl. Mech. Eng., **190**(4041), pp. 5427–5464.
[64] Miehe, C., Schröder, J., and Becker, M., 2002, "Computational Homogenization Analysis in Finite Elasticity: Material and Structural Instabilities on the Micro- and Macro-Scales of Periodic Composites and Their Interaction," Comput. Methods Appl. Mech. Eng., **191**(44), pp. 4971–5005.
[65] Kouznetsova, V., Brekelmans, W. A. M., and Baaijens, F. P. T., 2001, "An Approach to Micro-Macro Modeling of Heterogeneous Materials," Comput. Mech., **27**(1), pp. 37–48.
[66] Milton, G., 2001, *Theory of Composites*, Cambridge University Press, Cambridge, UK.
[67] Floquet, G., 1883, "Sur les équations différentielles linéaires à coefficients périodiques," Ann. Ec. Norm. Supér., **12**, p. 4788.
[68] Bloch, F., 1928, "Über die Quantenmechanik der Elektronen in Kristallgittern," Z. Phys., **52**, pp. 550–600.
[69] Krödel, S., Delpero, T., Bergamini, A., Ermanni, P., and Kochmann, D. M., 2014, "3D Auxetic Microlattices With Independently-Controllable Acoustic Band Gaps and Quasi-Static Elastic Moduli," Adv. Eng. Mater., **16**(4), pp. 357–363.
[70] Willis, J., 1981, "Variational and Related Methods for the Overall Properties of Composites," Adv. Appl. Mech., **21**, pp. 1–78.
[71] Willis, J., 1981, "Variational Principles for Dynamic Problems for Inhomogeneous Elastic Media," Wave Motion, **3**(1), pp. 1–11.
[72] Willis, J., 1997, "Dynamics of Composites," *Continuum Micromechanics*, P. Suquet, ed., Springer, New York, pp. 265–290.
[73] Milton, G., and Willis, J., 2007, "On Modifications of Newton's Second Law and Linear Continuum Elastodynamics," Proc. R. Soc. A, **463**(2079), pp. 855–880.
[74] Willis, J., 2009, "Exact Effective Relations for Dynamics of a Laminated Body," Mech. Mater., **41**(4), pp. 385–393.
[75] Willis, J., 2011, "Effective Constitutive Relations for Waves in Composites and Metamaterials," Proc. R. Soc. A, **467**(2131), pp. 1865–1879.
[76] Norris, A., Shuvalov, A., and Kutsenko, A., 2012, "Analytical Formulation of Three-Dimensional Dynamic Homogenization for Periodic Elastic Systems," Proc. R. Soc. A, **468**(2142), pp. 1629–1651.
[77] Pham, K., Kouznetsova, V., and Geers, M., 2013, "Transient Computational Homogenization for Heterogeneous Materials Under Dynamic Excitation," J. Mech. Phys. Solids, **61**(11), pp. 2125–2146.
[78] Liu, C., and Reina, C., 2015, "Computational Homogenization of Heterogeneous Media Under Dynamic Loading," preprint arXiv:1510.02310.
[79] Hill, R., 1957, "On Uniqueness and Stability in the Theory of Finite Elastic Strain," J. Mech. Phys. Solids, **5**(4), pp. 229–241.
[80] Hill, R., 1961, "Uniqueness in General Boundary-Value Problems for Elastic or Inelastic Solids," J. Mech. Phys. Solids, **9**(2), pp. 114–130.
[81] Ball, J. M., 1976, "Convexity Conditions and Existence Theorems in Nonlinear Elasticity," Arch. Ration. Mech. Anal., **63**(4), pp. 337–403.
[82] Lyapunov, A., 1892, "The General Problem of the Stability of Motion," Ph.D. thesis, University of Kharkov, Kharkov, Russia (in Russian).
[83] Lyapunov, A., 1966, *The General Problem of the Stability of Motion*, Academic Press, New York.
[84] Koiter, W., 1965, "The Energy Criterion of Stability for Continuous Elastic Bodies," Proc. K. Ned. Acad. Wet. B, **868**, pp. 178–202.
[85] Kochmann, D. M., and Drugan, W. J., 2011, "Infinitely Stiff Composite Via a Rotation-Stabilized Negative-Stiffness Phase," Appl. Phys. Lett., **99**(1), p. 011909.
[86] Ziegler, H., 1953, "Linear Elastic Stability," Z. Angew. Math. Phys., **4**(3), pp. 167–185.
[87] Ortiz, M., and Stainier, L., 1999, "The Variational Formulation of Viscoplastic Constitutive Updates," Comput. Methods Appl. Mech. Eng., **171**(34), pp. 419–444.
[88] Bazant, Z. P., 2000, "Structural Stability," Int. J. Solids Struct., **37**(12), pp. 55–67.
[89] Ning, X., and Pellegrino, S., 2015, "Imperfection-Insensitive Axially Loaded Thin Cylindrical Shells," Int. J. Solids Struct., **62**, pp. 39–51.
[90] Thomson, W. L. K., 1856, "Elements of a Mathematical Theory of Elasticity," Philos. Trans. R. Soc. London, **146**, pp. 481–498.

[91] Van Hove, L., 1947, "Sur l'extension de la condition de legendre du calcul des variations aux intégrales multiples à plusieurs fonctions inconnues," Proc. Ned. Akad. Wet., **50**, p. 1823.
[92] Mandel, J., 1962, "Ondes plastique dans un milieu indéfini à trois dimensions," J. Mech., **1**, pp. 3–30.
[93] Mandel, J., 1966, "Conditions de stabilité et postulat de drucker," *Rheology and Solid Mechanics*, J. Kravtchenko and M. Sirieys, eds., Springer, Berlin, pp. 58–68.
[94] Kochmann, D. M., 2012, "Stability Criteria for Continuous and Discrete Elastic Composites and the Influence of Geometry on the Stability of a Negative-Stiffness Phase," Phys. Status Solidi B, **249**(7), pp. 1399–1411.
[95] Pearson, C. E., 1956, "General Theory of Elastic Stability," Q. Appl. Math., **14**, pp. 133–144.
[96] Kochmann, D. M., and Drugan, W. J., 2012, "Analytical Stability Conditions for Elastic Composite Materials With a Non-Positive-Definite Phase," Proc. R. Soc. A, **468**(2144), pp. 2230–2254.
[97] Triantafyllidis, N., and Maker, B., 1985, "On the Comparison Between Microscopic and Macroscopic Instability Mechanisms in a Class of Fiber-Reinforced Composites," ASME J. Appl. Mech., **52**(4), pp. 794–800.
[98] Kochmann, D., and Drugan, W., 2009, "Dynamic Stability Analysis of an Elastic Composite Material Having a Negative-Stiffness Phase," J. Mech. Phys. Solids, **57**(7), pp. 1122–1138.
[99] Kochmann, D. M., and Milton, G. W., 2014, "Rigorous Bounds on the Effective Moduli of Composites and Inhomogeneous Bodies With Negative-Stiffness Phases," J. Mech. Phys. Solids, **71**, pp. 46–63.
[100] Lakes, R., 1999, *Viscoelastic Solids* (CRC Mechanical Engineering Series), CRC Press, Boca Raton, FL.
[101] Fritzen, F., and Kochmann, D. M., 2014, "Material Instability-Induced Extreme Damping in Composites: A Computational Study," Int. J. Solids Struct., **51**(23–24), pp. 4101–4112.
[102] Lakes, R., 1993, "Materials With Structural Hierarchy," Nature, **361**(6412), pp. 511–515.
[103] Kim, H., Swan, C., and Lakes, R., 2002, "Computational Studies on High-Stiffness, High-Damping SiC–InSn Particulate Reinforced Composites," Int. J. Solids Struct., **39**(23), pp. 5799–5812.
[104] Meaud, J., Sain, T., Hulbert, G., and Waas, A., 2013, "Analysis and Optimal Design of Layered Composites With High Stiffness and High Damping," Int. J. Solids Struct., **50**(9), pp. 1342–1353.
[105] Meaud, J., Sain, T., Yeom, B., Park, S. J., Shoultz, A. B., Hulbert, G., Ma, Z.-D., Kotov, N. A., Hart, A. J., Arruda, E. M., and Waas, A. M., 2014, "Simultaneously High Stiffness and Damping in Nanoengineered Microtruss Composites," ACS Nano, **8**(4), pp. 3468–3475.
[106] Wang, Y. C., and Lakes, R. S., 2004, "Extreme Stiffness Systems Due to Negative Stiffness Elements," Am. J. Phys., **72**(1), pp. 40–50.
[107] Wojnar, C. S., and Kochmann, D. M., 2014, "A Negative-Stiffness Phase in Elastic Composites Can Produce Stable Extreme Effective Dynamic But Not Static Stiffness," Philos. Mag., **94**(6), pp. 532–555.
[108] Liu, Z., Zhang, X., Mao, Y., Zhu, Y., Yang, Z., Chan, C., and Sheng, P., 2000, "Locally Resonant Sonic Materials," Science, **289**(5485), pp. 1734–1736.
[109] Sheng, P., Zhang, X., Liu, Z., and Chan, C., 2003, "Locally Resonant Sonic Materials," Physica B, **338**(1–4), pp. 201–205.
[110] Fang, N., Xi, D., Xu, J., Ambati, M., Srituravanich, W., Sun, C., and Zhang, X., 2006, "Ultrasonic Metamaterials With Negative Modulus," Nat. Mater., **5**(6), pp. 452–456.
[111] Platus, D. L., 1992, "Negative Stiffness-Mechanism Vibration Isolation System," Proc. SPIE, **1619**, p. 44–54.
[112] Platus, D. L., and Ferry, D. K., 2007, "Negative-Stiffness Vibration Isolation Improves Reliability of Nanoinstrumentation," Laser Focus World, **43**(10), pp. 107–109.
[113] Lee, C.-M., Goverdovskiy, V., and Temnikov, A., 2007, "Design of Springs With Negative Stiffness to Improve Vehicle Driver Vibration Isolation," J. Sound Vib., **302**(4–5), pp. 865–874.
[114] Sarlis, A. A., Pasala, D. T. R., Constantinou, M. C., Reinhorn, A. M., Nagarajaiah, S., and Taylor, D. P., 2016, "Negative Stiffness Device for Seismic Protection of Structures: Shake Table Testing of a Seismically Isolated Structure," J. Struct. Eng., **142**(5), p. 04016005.
[115] Moore, B., Jaglinski, T., Stone, D. S., and Lakes, R. S., 2006, "Negative Incremental Bulk Modulus in Foams," Philos. Mag. Lett., **86**(10), pp. 651–659.
[116] Estrin, Y., Dyskin, A. V., Pasternak, E., Schaare, S., Stanchits, S., and Kanel-Belov, A. J., 2004, "Negative Stiffness of a Layer With Topologically Interlocked Elements," Scr. Mater., **50**(2), pp. 291–294.
[117] Cherkaev, A., Cherkaev, E., and Slepyan, L., 2005, "Transition Waves in Bistable Structures. I. Delocalization of Damage," J. Mech. Phys. Solids, **53**(2), pp. 383–405.
[118] Kashdan, L., Seepersad, C. C., Haberman, M., and Wilson, P. S., 2012, "Design, Fabrication, and Evaluation of Negative Stiffness Elements Using SLS," Rapid Prototyping J., **18**(3), pp. 194–200.
[119] Klatt, T., and Haberman, M. R., 2013, "A Nonlinear Negative Stiffness Metamaterial Unit Cell and Small-on-Large Multiscale Material Model," J. Appl. Phys., **114**(3), p. 033503.
[120] Matthews, J., Klatt, T., Morris, C., Seepersad, C. C., Haberman, M., and Shahan, D., 2016, "Hierarchical Design of Negative Stiffness Metamaterials Using a Bayesian Network Classifier," ASME J. Mech. Des., **138**(4), p. 041404.
[121] Konarski, S. G., Hamilton, M. F., and Haberman, M. R., 2014, "Elastic Nonlinearities and Wave Distortion in Heterogeneous Materials Containing Constrained Negative Stiffness Inclusions," Eighth International Congress on Advanced Electromagnetic Materials in Microwaves and Optics (METAMATERIALS), Lyngby, Denmark, Aug. 25–28, pp. 130–132.
[122] Novak, I., and Truskinovsky, L., 2015, "Nonaffine Response of Skeletal Muscles on the 'Descending Limb'," Math. Mech. Solids, **20**(6), pp. 697–720.
[123] Caruel, M., Allain, J.-M., and Truskinovsky, L., 2013, "Muscle as a Metamaterial Operating Near a Critical Point," Phys. Rev. Lett., **110**, p. 248103.
[124] Snyder, K. V., Brownell, W. E., and Sachs, F., 1999, "Negative Stiffness of the Outer Hair Cell Lateral Wall," Biophys. J., **76**(1), p. A60.
[125] Hashin, Z., and Shtrikman, S., 1963, "A Variational Approach to the Theory of the Elastic Behaviour of Multiphase Materials," J. Mech. Phys. Solids, **11**(2), pp. 127–140.
[126] Novikov, V. V., and Wojciechowski, K. W., 2005, "Extreme Viscoelastic Properties of Composites of Strongly Inhomogeneous Structures Due to Negative Stiffness Phases," Phys. Status Solidi B, **242**(3), pp. 645–652.
[127] Wang, Y. C., and Lakes, R. S., 2001, "Extreme Thermal Expansion, Piezoelectricity, and Other Coupled Field Properties in Composites With a Negative Stiffness Phase," J. Appl. Phys., **90**(12), pp. 6458–6465.
[128] Wang, Y.-C., Ko, C.-C., and Chang, K.-W., 2015, "Anomalous Effective Viscoelastic, Thermoelastic, Dielectric, and Piezoelectric Properties of Negative-Stiffness Composites and Their Stability," Phys. Status Solidi B, **252**(7), pp. 1640–1655.
[129] Chronopoulos, D., Antoniadis, I., Collet, M., and Ichchou, M., 2015, "Enhancement of Wave Damping Within Metamaterials Having Embedded Negative Stiffness Inclusions," Wave Motion, **58**, pp. 165–179.
[130] Jeeva, L. L., Choi, J. B., and Lee, T., 2014, "Improvement of Viscoelastic Damping by Using Manganese Bronze With Indium," Mech. Time-Depend. Mater., **18**(1), pp. 217–227.
[131] Wang, Y. C., Ludwigson, M., and Lakes, R. S., 2004, "Deformation of Extreme Viscoelastic Metals and Composites," Mater. Sci. Eng. A, **370**(1–2), pp. 41–49.
[132] Prasad, J., and Diaz, A. R., 2009, "Viscoelastic Material Design With Negative Stiffness Components Using Topology Optimization," Struct. Multidiscip. Optim., **38**(6), pp. 583–597.
[133] Lakes, R. S., and Drugan, W. J., 2002, "Dramatically Stiffer Elastic Composite Materials Due to a Negative Stiffness phase?," J. Mech. Phys. Solids, **50**(5), pp. 979–1009.
[134] Drugan, W. J., 2007, "Elastic Composite Materials Having a Negative Stiffness Phase Can Be Stable," Phys. Rev. Lett., **98**(5), p. 055502.
[135] Hoang, T. M., and Drugan, W. J., 2016, "Tailored Heterogeneity Increases Overall Stability Regime of Composites Having a Negative-Stiffness Inclusion," J. Mech. Phys. Solids, **88**, pp. 123–149.
[136] Wojnar, C. S., and Kochmann, D. M., 2014, "Stability of Extreme Static and Dynamic Bulk Moduli of an Elastic Two-Phase Composite Due to a Non-Positive-Definite Phase," Phys. Status Solidi B, **251**(2), pp. 397–405.
[137] Wang, Y. C., and Lakes, R., 2004, "Negative Stiffness-Induced Extreme Viscoelastic Mechanical Properties: Stability and Dynamics," Philos. Mag., **84**(35), pp. 3785–3801.
[138] Wang, Y. C., and Lakes, R., 2005, "Stability of Negative Stiffness Viscoelastic Systems," Q. Appl. Math., **63**(1), pp. 34–55.
[139] Wang, Y. C., Swadener, J. G., and Lakes, R. S., 2006, "Two-Dimensional Viscoelastic Discrete Triangular System With Negative-Stiffness Components," Philos. Mag. Lett., **86**(2), pp. 99–112.
[140] Wang, Y. C., 2007, "Influences of Negative Stiffness on a Two-Dimensional Hexagonal Lattice Cell," Philos. Mag., **87**(24), pp. 3671–3688.
[141] Wang, Y.-C., Swadener, J. G., and Lakes, R. S., 2007, "Anomalies in Stiffness and Damping of a 2D Discrete Viscoelastic System Due to Negative Stiffness Components," Thin Solid Films, **515**(6), pp. 3171–3178.
[142] Kochmann, D. M., 2014, "Stable Extreme Damping in Viscoelastic Two-Phase Composites With Non-Positive-Definite Phases Close to the Loss of Stability," Mech. Res. Commun., **58**, pp. 36–45.
[143] Wang, Y. C., and Lakes, R. S., 2004, "Stable Extremely-High-Damping Discrete Viscoelastic Systems Due to Negative Stiffness Elements," Appl. Phys. Lett., **84**(22), pp. 4451–4453.
[144] Wang, Y.-C., and Ko, C.-C., 2010, "Stability of Viscoelastic Continuum With Negative-Stiffness Inclusions in the Low-Frequency Range," Phys. Status Solidi B, **250**(10), pp. 2070–2079.
[145] Junker, P., and Kochmann, D. M., 2017, "Damage-Induced Mechanical Damping in Phase-Transforming Composites Materials," Int. J. Solids Struct., **113–114**, pp. 132–146.
[146] Kapitza, P. L., 1951, "Dynamic Stability of a Pendulum When Its Point of Suspension Vibrates," Sov. Phys. JETP, **21**, pp. 588–592.
[147] Kapitza, P. L., 1951, "Pendulum With a Vibrating Suspension," Usp. Fiz. Nauk, **44**, pp. 7–15.
[148] Kochmann, D. M., and Drugan, W. J., 2016, "An Infinitely-Stiff Elastic System Via a Tuned Negative-Stiffness Component Stabilized by Rotation-Produced Gyroscopic Forces," Appl. Phys. Lett., **108**(26), p. 261904.
[149] Lakes, R. S., 2012, "Stable Singular or Negative Stiffness Systems in the Presence of Energy Flux," Philos. Mag. Lett., **92**(5), pp. 226–234.
[150] Jaglinski, T., and Lakes, R. S., 2004, "Anelastic Instability in Composites With Negative Stiffness Inclusions," Philos. Mag. Lett., **84**(12), pp. 803–810.
[151] Jaglinski, T., Stone, D., and Lakes, R. S., 2005, "Internal Friction Study of a Composite With a Negative Stiffness Constituent," J. Mater. Res., **20**(9), pp. 2523–2533.
[152] Jaglinski, T., Frascone, P., Moore, B., Stone, D. S., and Lakes, R. S., 2006, "Internal Friction Due to Negative Stiffness in the Indium-Thallium Martensitic Phase Transformation," Philos. Mag., **86**(27), pp. 4285–4303.

[153] Dong, L., Stone, D., and Lakes, R., 2011, "Giant Anelastic Responses in ($BaZrO_3$-ZnO)-$BaTiO_3$ Composite Materials," EPL, **93**(6), p. 66003.
[154] Dong, L., Stone, D. S., and Lakes, R. S., 2011, "Extreme Anelastic Responses in $Zn_{80}Al_{20}$ Matrix Composite Materials Containing $BaTiO_3$ Inclusion," Scr. Mater., **65**(4), pp. 288–291.
[155] Dong, L., Stone, D. S., and Lakes, R. S., 2011, "Viscoelastic Sigmoid Anomalies in $BaZrO_3$-$BaTiO_3$ Near Phase Transformations Due to Negative Stiffness Heterogeneity," J. Mater. Res., **26**(11), pp. 1446–1452.
[156] Skandani, A. A., Ctvrtlik, R., and Al-Haik, M., 2014, "Nanocharacterization of the Negative Stiffness of Ferroelectric Materials," Appl. Phys. Lett., **105**(8), p. 082906.
[157] Romao, C. P., and White, M. A., 2016, "Negative Stiffness in ZrW_2O_8 Inclusions as a Result of Thermal Stress," Appl. Phys. Lett., **109**(3), p. 031902.
[158] le Graverend, J.-B., Wojnar, C. S., and Kochmann, D. M., 2015, "Broadband Electromechanical Spectroscopy: Characterizing the Dynamic Mechanical Response of Viscoelastic Materials Under Temperature and Electric Field Control in a Vacuum Environment," J. Mater. Sci., **50**(10), pp. 3656–3685.
[159] Mullin, T., Deschanel, S., Bertoldi, K., and Boyce, M. C., 2007, "Pattern Transformation Triggered by Deformation," Phys. Rev. Lett., **99**(8), p. 084301.
[160] Zhang, Y., Matsumoto, E. A., Peter, A., Lin, P. C., Kamien, R. D., and Yang, S., 2008, "One-Step Nanoscale Assembly of Complex Structures Via Harnessing of an Elastic Instability," Nano Letters, **8**(4), pp. 1192–1196.
[161] Michel, J., Lopez-Pamies, O., Castañeda, P. P., and Triantafyllidis, N., 2007, "Microscopic and Macroscopic Instabilities in Finitely Strained Porous Elastomers," J. Mech. Phys. Solids, **55**(5), pp. 900–938.
[162] Triantafyllidis, N., Nestorovic, M. D., and Schraad, M. W., 2006, "Failure Surfaces for Finitely Strained Two-Phased Periodic Solids Under General In-Plane Loading," ASME J. Appl. Mech., **73**(3), pp. 505–515.
[163] Bertoldi, K., Reis, P. M., Willshaw, S., and Mullin, T., 2010, "Negative Poisson's Ratio Behavior Induced by an Elastic Instability," Adv. Mater., **22**(3), pp. 361–366.
[164] Babaee, S., Shim, J., Weaver, J., Patel, N., and Bertoldi, K., 2013, "3D Soft Metamaterials With Negative Poisson's Ratio," Adv. Mater., **25**(36), pp. 5044–5049.
[165] Liu, J., Gu, T., Shan, S., Kang, S., Weaver, J., and Bertoldi, K., 2016, "Harnessing Buckling to Design Architected Materials That Exhibit Effective Negative Swelling," Adv. Mater., **28**(31), pp. 6619–6624.
[166] Kang, S., Shan, S., Noorduin, W., Khan, M., Aizenberg, J., and Bertoldi, K., 2013, "Buckling-Induced Reversible Symmetry Breaking and Amplification of Chirality Using Supported Cellular Structures," Adv. Mater., **25**(24), pp. 3380–3385.
[167] Cao, B., Wu, G., Xia, Y., and Yang, S., 2016, "Buckling Into Single-Handed Chiral Structures From *p*H-Sensitive Hydrogel Membranes," Extreme Mech. Lett., **7**, pp. 49–54.
[168] Wu, G., Xia, Y., and Yang, S., 2014, "Buckling, Symmetry Breaking, and Cavitation in Periodically Micro-Structured Hydrogel Membranes," Soft Matter, **10**(9), pp. 1392–1399.
[169] Lazarus, A., and Reis, P., 2015, "Soft Actuation of Structured Cylinders Through Auxetic Behavior," Adv. Eng. Mater., **17**(6), pp. 815–820.
[170] Yang, D., Mosadegh, B., Ainla, A., Lee, B., Khashai, F., Suo, Z., Bertoldi, K., and Whitesides, G., 2015, "Buckling of Elastomeric Beams Enables Actuation of Soft Machines," Adv. Mater., **27**(41), pp. 6323–6327.
[171] Li, J., Shim, J., Deng, J., Overvelde, J., Zhu, X. B. K., and Yang, S., 2012, "Switching Periodic Membranes Via Pattern Transformation and Shape Memory Effect," Soft Matter, **8**(40), pp. 10322–10328.
[172] Zhu, X., Wu, G., Dong, R., Chen, C., and Yang, S., 2012, "Capillarity Induced Instability in Responsive Hydrogel Membranes With Periodic Hole Array," Soft Matter, **8**(31), pp. 8088–8093.
[173] Bertoldi, K., and Boyce, M. C., 2008, "Mechanically-Triggered Transformations of Phononic Band Gaps in Periodic Elastomeric Structures," Phys. Rev. B, **77**(5), p. 052105.
[174] Shan, S., Kang, S., Wang, P., Qu, C., Shian, S., Chen, E., and Bertoldi, K., 2014, "Harnessing Multiple Folding Mechanisms in Soft Periodic Structures for Tunable Control of Elastic Waves," Adv. Funct. Mater., **24**(31), p. 4935.
[175] Raney, J., and Lewis, J., 2015, "Printing Mesoscale Architectures," MRS Bull., **40**(11), pp. 943–950.
[176] Williams, F., and Anderson, M., 1983, "Incorporation of Lagrangian Multipliers Into an Algorithm for Finding Exact Natural Frequencies or Critical Buckling Loads," Int. J. Mech. Sci., **25**(8), pp. 579–584.
[177] Triantafyllidis, N., and Schnaidt, W., 1993, "Comparison of Microscopic and Macroscopic Instabilities in a Class of Two-Dimensional Periodic Composites," J. Mech. Phys. Solids, **41**(9), pp. 1533–1565.
[178] Bertoldi, K., Boyce, M. C., Deschanel, S., Prange, S. M., and Mullin, T., 2008, "Mechanics of Deformation-Triggered Pattern Transformations and Superelastic Behavior in Periodic Elastomeric Structures," J. Mech. Phys. Solids, **56**(8), pp. 2642–2668.
[179] Ning, X., and Pellegrino, S., 2015, "Buckling Analysis of Axially Loaded Corrugated Cylindrical Shells," AIAA Paper No. 2015-1435.
[180] Shim, J., Shan, S., Kosmrlj, A., Kang, S., Chen, E., Weaver, J., and Bertoldi, K., 2013, "Harnessing Instabilities for Design of Soft Reconfigurable Auxetic/Chiral Materials," Soft Matter, **9**(34), pp. 8198–8202.
[181] Kang, S. H., Shan, S., Košmrlj, A., Noorduin, W. L., Shian, S., Weaver, J. C., Clarke, D. R., and Bertoldi, K., 2014, "Complex Ordered Patterns in Mechanical Instability Induced Geometrically Frustrated Triangular Cellular Structures," Phys. Rev. Lett., **112**(9), p. 098701.
[182] Javid, F., Liu, J., Shim, J., Weaver, J. C., Shanian, A., and Bertoldi, K., 2016, "Mechanics of Instability-Induced Pattern Transformations in Elastomeric Porous Cylinders," J. Mech. Phy. Solids, **96**, pp. 1–17.
[183] Hong, W., Liu, Z., and Suo, Z., 2009, "Inhomogeneous Swelling of a Gel in Equilibrium With a Solvent and Mechanical Load," Int. J. Solids Struct., **46**(17), pp. 3282–3289.
[184] Tipton, C., Han, E., and Mullin, T., 2012, "Magneto-Elastic Buckling of a Soft Cellular Solid," Soft Matter, **8**(26), pp. 6880–6883.
[185] Zhu, X., 2011, "Design and Fabrication of Photonic Microstructures by Holographic Lithography and Pattern Transformation," Ph.D. thesis, University of Pennsylvania, Philadelphia, PA.
[186] Rivlin, R. S., 1948, "Large Elastic Deformations of Isotropic Materials. II. Some Uniqueness Theorems for Pure, Homogeneous Deformation," Philos. Trans. R. Soc. London A, **240**(822), pp. 491–508.
[187] Overvelde, J. T. B., Dykstra, D. M. J., de Rooij, R., Weaver, J., and Bertoldi, K., 2016, "Tensile Instability in a Thick Elastic Body," Phys. Rev. Lett., **117**(9), p. 094301.
[188] Bertoldi, K., and Boyce, M. C., 2008, "Wave Propagation and Instabilities in Monolithic and Periodically Structured Elastomeric Materials Undergoing Large Deformations," Phys. Rev. B, **78**(18), p. 184107.
[189] Rafsanjani, A., Akbarzadeh, A., and Pasini, D., 2015, "Snapping Mechanical Metamaterials Under Tension," Adv. Mater., **27**(39), pp. 5931–5935.
[190] Rafsanjani, A., and Pasini, D., 2016, "Bistable Auxetic Mechanical Metamaterials Inspired by Ancient Geometric Motifs," Extreme Mech. Lett., **9**(Pt. 2), pp. 291–296.
[191] Zhang, Y., Yan, Z., Nan, K., Xiao, D., Liu, Y., Luan, H., Fu, H., Wang, X., Yang, Q., Wang, J., Ren, W., Si, H., Liu, F., Yang, L., Li, H., Wang, J., Guo, X., Luo, H., Wang, L., Huang, Y., and Rogers, J. A., 2015, "A Mechanically Driven Form of Kirigami as a Route to 3D Mesostructures in Micro/Nanomembranes," Proc. Natl. Acad. Sci. U.S.A., **112**(38), p. 11757.
[192] Rafsanjani, A., and Bertoldi, K., 2017, "Buckling-Induced Kirigami," Phys. Rev. Lett., **118**(8), p. 084301.
[193] Song, Z., Wang, X., Lv, C., An, Y., Liang, M., Ma, T., He, D., Zheng, Y.-J., Huang, S.-Q., Yu, H., and Jiang, H., 2015, "Kirigami-Based Stretchable Lithium-Ion Batteries," Sci. Rep., **5**(1), p. 10988.
[194] Shyu, T. C., Damasceno, P. F., Dodd, P. M., Lamoureux, A., Xu, L., Shlian, M., Shtein, M., Glotzer, S. C., and Kotov, N. A., 2015, "A Kirigami Approach to Engineering Elasticity in Nanocomposites Through Patterned Defects," Nat. Mater., **14**, p. 785.
[195] Blees, K., Barnard, A. W., Rose, P. A., Roberts, S. P., McGill, K. L., Huang, P. Y., Ruyack, A. R., Kevek, J. W., Kobrin, B., Muller, D. A., and McEuen, P. L., 2015, "Graphene Kirigami," Nature, **524**(7564), p. 204.
[196] Lamoureux, A., Lee, K., Shlian, M., Forrest, S. R., and Shtein, M., 2015, "Dynamic Kirigami Structures for Integrated Solar Tracking," Nat. Comm., **6**, p. 8092.
[197] Wu, C., Wang, X., Lin, L., Guo, H., and Wang, Z. L., 2016, "Paper-Based Triboelectric Nanogenerators Made of Stretchable Interlocking Kirigami Patterns," ACS Nano, **10**(4), p. 4652.
[198] Isobe, M., and Okumura, K., 2016, "Initial Rigid Response and Softening Transition of Highly Stretchable Kirigami Sheet Materials," Sci. Rep., **6**, p. 24758.
[199] Yan, Z., Zhang, F., Wang, J., Liu, F., Guo, X., Nan, K., Lin, Q., Gao, M., Xiao, D., Shi, Y., Qiu, Y., Luan, H., Kim, J. H., Wang, Y., Luo, H., Han, M., Huang, Y., Zhang, Y., and Rogers, J. A., 2016, "Controlled Mechanical Buckling for Origami-Inspired Construction of 3D Microstructures in Advanced Materials," Adv. Funct. Mater., **26**(16), pp. 2629–2639.
[200] Neville, R., Scarpa, F., and Pirrera, A., 2016, "Shape Morphing Kirigami Mechanical Metamaterials," Sci. Rep., **6**, p. 31067.
[201] Coulais, C., Teomy, E., de Reus, K., Shokef, Y., and van Hecke, M., 2016, "Combinatorial Design of Textured Mechanical Metamaterials," Nature, **535**(7653), pp. 529–532.
[202] Hussein, M., Leamy, M., and Ruzzene, M., 2014, "Dynamics of Phononic Materials and Structures: Historical Origins, Recent Progress and Future Outlook," Appl. Mech. Rev., **66**(4), p. 040802.
[203] Khelif, A., Choujaa, A., Benchabane, S., Djafari-Rouhani, B., and Laude, V., 2004, "Guiding and Bending of Acoustic Waves in Highly Confined Phononic Crystal Waveguides," Appl. Phys. Lett., **84**(22), pp. 4400–4402.
[204] Kafesaki, M., Sigalas, M. M., and Garcia, N., 2000, "Frequency Modulation in the Transmittivity of Wave Guides in Elastic-Wave Band-Gap Materials," Phys. Rev. Lett., **85**(19), pp. 4044–4047.
[205] Cummer, S., and Schurig, D., 2007, "One Path to Acoustic Cloaking," New J. Phys., **9**, p. 45.
[206] Elser, D., Andersen, U. L., Korn, A., Glöckl, O., Lorenz, S., Marquardt, C., and Leuchs, G., 2006, "Reduction of Guided Acoustic Wave Brillouin Scattering in Photonic Crystal Fibers," Phys. Rev. Lett., **97**(13), p. 133901.
[207] Elnady, T., Elsabbagh, A., Akl, W., Mohamady, O., Garcia-Chocano, V. M., Torrent, D., Cervera, F., and Sánchez-Dehesa, J., 2009, "Quenching of Acoustic Bandgaps by Flow Noise," Appl. Phys. Lett., **94**(13), p. 134104.
[208] Casadei, F., Dozio, L., Ruzzene, M., and Cunefare, K., 2010, "Periodic Shunted Arrays for the Control of Noise Radiation in an Enclosure," J. Sound Vib., **329**(18), p. 3632.
[209] Airoldi, L., and Ruzzene, M., 2011, "Design of Tunable Acoustic Metamaterials Through Periodic Arrays of Resonant Shunted Piezos," New J. Phys., **13**(11), p. 113010.
[210] Casadei, F., Beck, B., Cunefare, K. A., and Ruzzene, M., 2012, "Vibration Control of Plates Through Hybrid Configurations of Periodic Piezoelectric Shunts," J. Intell. Mater. Syst. Struct., **23**(10), pp. 1169–1177.
[211] Kittel, C., 1967, "Introduction to Solid State Physics," Am. J. Phys., **35**(6), pp. 547–548.

[212] Kinra, V. K., and Ker, E. L., 1983, "An Experimental Investigation of Pass Bands and Stop Bands in Two Periodic Particulate Composites," Int. J. Solids Struct., **19**(5), pp. 393–410.
[213] Kafesaki, M., Sigalas, M. M., and Economou, E. N., 1995, "Elastic Wave Band Gaps in 3-D Periodic Polymer Matrix Composites," Solid State Commun., **96**(5), pp. 285–289.
[214] Zhang, X., Liu, Z., Liu, Y., and Wu, F., 2003, "Elastic Wave Band Gaps for Three-Dimensional Phononic Crystals With Two Structural Units," Phys. Lett. A, **313**(56), pp. 455–460.
[215] Page, J., Yang, S., Cowan, M., Liu, Z., Chan, C., and Sheng, P., 2003, "3D Phononic Crystals," *Wave Scattering in Complex Media: From Theory to Applications* (NATO Science Series), Vol. 107, B. van Tiggelen and S. Skipetrov, eds., Springer, Dordrecht, The Netherlands, pp. 282–307.
[216] Yang, S. X., Page, J. H., Liu, Z. Y., Cowan, M. L., Chan, C. T., and Sheng, P., 2004, "Focusing of Sound in a 3D Phononic Crystal," Phys. Rev. Lett., **93**(2), p. 024301.
[217] Sainidou, R., Djafari-Rouhani, B., Pennec, Y., and Vasseur, J. O., 2006, "Locally Resonant Phononic Crystals Made of Hollow Spheres or Cylinders," Phys. Rev. B, **73**(2), p. 024302.
[218] Wang, P., Shim, J., and Bertoldi, K., 2013, "Effects of Geometric and Material Non-Linearities on the Tunable Response of Phononic Crystals," Phys. Rev. B, **88**(1), p. 014304.
[219] Mousanezhad, D., Babaee, S., Ghosh, R., Mahdi, E., Bertoldi, K., and Vaziri, A., 2015, "Honeycomb Phononic Crystals With Self-Similar Hierarchy," Phys. Rev. B, **92**(10), p. 104304.
[220] Babaee, S., Wang, P., and Bertoldi, K., 2015, "Three-Dimensional Adaptive Soft Phononic Crystals," J. Appl. Phys., **117**(24), p. 244903.
[221] Celli, P., Gonella, S., Tajeddini, V., Muliana, A., Ahmed, S., and Ounaies, Z., 2017, "Wave Control Through Soft Microstructural Curling: Bandgap Shifting, Reconfigurable Anisotropy and Switchable Chirality," Smart Mater. Struct., **26**(3), p. 035001.
[222] Brillouin, L., 1946, *Wave Propagation in Periodic Structures*, Dover Publications, Mineola, NY.
[223] Parnell, W., 2007, "Effective Wave Propagation in a Prestressed Nonlinear Elastic Composite Bar," IMA J. Appl. Math., **72**(2), pp. 223–244.
[224] Parnell, W., 2010, "Pre-Stressed Viscoelastic Composites: Effective Incremental Moduli and Band-Gap Tuning," AIP Conf. Proc., **1281**(1), pp. 837–840.
[225] Pal, R., Rimoli, J., and Ruzzene, M., 2016, "Effect of Large Deformation Pre-Loads on the Wave Properties of Hexagonal Lattices," Smart Mater. Struct., **25**, p. 054010.
[226] Gibson, L., Ashby, M., Zhang, J., and Triantafillou, T., 1989, "Failure Surfaces for Cellular Materials Under Multiaxial Loads—I: Modelling," Int. J. Solids Struct., **31**(9), pp. 635–663.
[227] Gibson, L., and Ashby, M., 1999, *Cellular Solids: Structure and Properties*, Cambridge University Press, Cambridge, UK.
[228] Papka, S., and Kyriakides, S., 1999, "Biaxial Crushing of Honeycombs: Part 1: Experiments," Int. J. Solids Struct., **36**(29), pp. 4367–4396.
[229] Papka, S., and Kyriakides, S., 1999, "In-Plane Biaxial Crushing of Honeycombs: Part II: Analysis," Int. J. Solids Struct., **36**(29), pp. 4397–4423.
[230] Chung, J., and Waas, A., 2001, "In-Plane Biaxial Crush Response of Polycarbonate Honeycombs," J. Eng. Mech., **127**(2), pp. 180–193.
[231] Ohno, N., Okumura, D., and Noguchi, H., 2002, "Microscopic Symmetric Bifurcation Condition of Cellular Solids Based on a Homogenization Theory of Finite Deformation," J. Mech. Phys. Solids, **50**(5), pp. 1125–1153.
[232] Combescure, C., Henry, P., and Elliott, R. S., 2016, "Post-Bifurcation and Stability of a Finitely Strained Hexagonal Honeycomb Subjected to Equi-Biaxial In-Plane Loading," Int. J. Solids Struct., **88–89**, pp. 296–318.
[233] Drugan, W., 2017, "Wave Propagation in Elastic and Damped Structures With Stabilized Negative-Stiffness Components," J. Mech. Phys. Solids, **106**, pp. 34–45.
[234] Puglisi, G., and Truskinovsky, L., 2000, "Mechanics of a Discrete Chain With Bi-Stable Elements," J. Mech. Phys. Solids, **48**(1), pp. 1–27.
[235] Cherkaev, A., Kouznetsov, A., and Panchenko, A., 2010, "Still States of Bistable Lattices, Compatibility, and Phase Transition," Continuum Mech. Thermodyn., **22**(6), pp. 421–444.
[236] Paulose, J., Meeussen, A. S., and Vitelli, V., 2015, "Selective Buckling Via States of Self-Stress in Topological Metamaterials," Proc. Natl. Acad. Sci., **112**(25), pp. 7639–7644.
[237] Shan, S., Kang, S. H., Raney, J., Wang, P., Fang, L., Candido, F., Lewis, J., and Bertoldi, K., 2015, "Multistable Architected Materials for Trapping Elastic Strain Energy," Adv. Mater., **27**(29), p. 4296.
[238] Restrepo, D., Mankame, N. D., and Zavattieri, P. D., 2015, "Phase Transforming Cellular Materials," Extreme Mech. Lett., **4**, pp. 52–60.
[239] Fraternali, F., Blesgen, T., Amendola, A., and Daraio, C., 2011, "Multiscale Mass-Spring Models of Carbon Nanotube Foams," J. Mech. Phys. Solids, **59**(1), pp. 89–102.
[240] Schaeffer, M., and Ruzzene, M., 2015, "Wave Propagation in Multistable Magneto-Elastic Lattices," Int. J. Solids Struct., **56–57**, pp. 78–95.
[241] Betts, D., Bowen, C., Kim, H., Gathercole, N., Clarke, C., and Inman, D., 2013, "Nonlinear Dynamics of a Bistable Piezoelectric-Composite Energy Harvester for Broadband Application," Eur. Phys. J. Spec. Top., **222**(7), pp. 1553–1562.
[242] Yang, K., Harne, R. L., Wang, K. W., and Huang, H., 2014, "Dynamic Stabilization of a Bistable Suspension System Attached to a Flexible Host Structure for Operational Safety Enhancement," J. Sound Vib., **333**(24), pp. 6651–6661.
[243] Harne, R. L., Thota, M., and Wang, K. W., 2013, "Concise and High-Fidelity Predictive Criteria for Maximizing Performance and Robustness of Bistable Energy Harvesters," Appl. Phys. Lett., **102**(5), p. 053903.
[244] Wu, Z. Z., Harne, R. L., and Wang, K. W., 2014, "Energy Harvester Synthesis Via Coupled Linear-Bistable System With Multistable Dynamics," ASME J. Appl. Mech., **81**(6), p. 061005.
[245] Johnson, D. R., Harne, R. L., and Wang, K. W., 2014, "A Disturbance Cancellation Perspective on Vibration Control Using a Bistable Snap-Through Attachment," ASME J. Vib. Acoust., **136**(3), p. 031006.
[246] Bolotin, V. V., 1965, "The Dynamic Stability of Elastic Systems. V. V. Bolotin. Translated from the Russian edition (Moscow, 1965) by V. I. Weingarten, L. B. Greszcuzuk, K. N. Trirogoff, and K. D. Gallegos. Holden-Day, San Francisco, CA, 1964. pp. xii + 451," Science, **148**(3670), pp. 627–628.
[247] Feeny, B. F., and Diaz, A. R., 2010, "Twinkling Phenomena in Snap-Through Oscillators," ASME J. Vib. Acoust., **132**(6), p. 061013.
[248] Nadkarni, N., Daraio, C., and Kochmann, D. M., 2014, "Dynamics of Periodic Mechanical Structures Containing Bistable Elastic Elements: From Elastic to Solitary Wave Propagation," Phys. Rev. E, **90**(2), p. 023204.
[249] Frenkel, Y., and Kontorova, T., 1938, "On Theory of Plastic Deformation and Twinning," Phys. Z. Sowjetunion, **13**, pp. 1–7.
[250] Braun, O. M., and Kivshar, Y. S., 1998, "Nonlinear Dynamics of the Frenkel Kontorova Model," Phys. Rep., **306**(12), pp. 1–108.
[251] Prandtl, L., 1928, "Ein gedankenmodell zur kinetischen theorie der festen krper," Z. Angew. Math. Mech., **8**(2), pp. 85–106.
[252] Benichou, I., and Givli, S., 2013, "Structures Undergoing Discrete Phase Transformation," J. Mech. Phys. Solids, **61**(1), pp. 94–113.
[253] Bour, E., 1862, "Théorie de la déformation des surfaces," J. Ec. Imp. Polytech. **19**, pp. 1–48.
[254] Scott, A. C., 1969, "A Nonlinear Klein-Gordon Equation," Am. J. Phys., **37**(1), pp. 52–61.
[255] Fermi, E., Pasta, J., and Ulam, S., 1965, "Studies of Nonlinear Problems (Los Alamos Report LA-1940)," *The Collected Papers of Enrico Fermi*, E. Segré, ed., University of Chicago Press, Chicago, IL.
[256] Boussinesq, J., 1877, "Essai sur la theorie des eaux courantes, memoires presentes par divers savants," Acad. Sci. Inst. Nat. France, **XXIII**, pp. 1–680.
[257] Korteweg, D. D. J., and de Vries, D. G., 1895, "XLI. On the Change of Form of Long Waves Advancing in a Rectangular Canal, and on a New Type of Long Stationary Waves," Philos. Mag., **39**(240), pp. 422–443.
[258] Chu, C., and James, R. D., 1995, "Analysis of Microstructures in Cu-14.0%Al-3.9%Ni by Energy Minimization," J. Phys. IV, **5**, pp. C8-143–C8-149.
[259] Jona, F., and Shirane, G., 1962, *Ferroelectric Crystals*, Pergamon Press, New York.
[260] Zhang, W., and Bhattacharya, K., 2005, "A Computational Model of Ferroelectric Domains. Part I: Model Formulation and Domain Switching," Acta Mater., **53**(1), pp. 185–198.
[261] Su, Y., and Landis, C. M., 2007, "Continuum Thermodynamics of Ferroelectric Domain Evolution: Theory, Finite Element Implementation, and Application to Domain Wall Pinning," J. Mech. Phys. Solids, **55**(2), pp. 280–305.
[262] Onuki, A., 2002, *Phase Transition Dynamics*, Cambridge University Press, Cambridge, UK.
[263] Bray, A. J., 2002, "Theory of Phase-Ordering Kinetics," Adv. Phys., **51**(2), pp. 481–587.
[264] Dye, D., 2015, "Shape Memory Alloys: Towards Practical Actuators," Nat. Mater., **14**, pp. 760–761.
[265] Fiebig, M., Lottermoser, T., Meier, D., and Trassin, M., 2016, "The Evolution of Multiferroics," Nat. Rev. Mater., **1**, p. 16046.
[266] Nadkarni, N., Daraio, C., Abeyaratne, R., and Kochmann, D. M., 2016, "Universal Energy Transport Law for Dissipative and Diffusive Phase Transitions," Phys. Rev. B, **93**(10), p. 104109.
[267] Nadkarni, N., Arrieta, A. F., Chong, C., Kochmann, D. M., and Daraio, C., 2016, "Unidirectional Transition Waves in Bistable Lattices," Phys. Rev. Lett., **116**(24), p. 244501.
[268] Allen, S. M., and Cahn, J. W., 1979, "A Microscopic Theory for Antiphase Boundary Motion and Its Application to Antiphase Domain Coarsening," Acta Metall., **27**(6), pp. 1085–1095.
[269] Zhang, W., and Bhattacharya, K., 2005, "A Computational Model of Ferroelectric Domains. Part II: Grain Boundaries and Defect Pinning," Acta Mater., **53**(1), pp. 199–209.
[270] Bishop, A. R., and Lewis, W. F., 1979, "A Theory of Intrinsic Coercivity in Narrow Magnetic Domain Wall Materials," J. Phys. C, **12**(18), p. 3811.
[271] Kashimori, Y., Kikuchi, T., and Nishimoto, K., 1982, "The Solitonic Mechanism for Proton Transport in a Hydrogen Bonded Chain," J. Chem. Phys., **77**(4), pp. 1904–1907.
[272] Peyrard, M., and Bishop, A. R., 1989, "Statistical Mechanics of a Nonlinear Model for DNA Denaturation," Phys. Rev. Lett., **62**(23), pp. 2755–2758.
[273] Thevamaran, R., Fraternali, F., and Daraio, C., 2014, "Multiscale Mass-Spring Model for High-Rate Compression of Vertically Aligned Carbon Nanotube Foams," ASME J. Appl. Mech., **81**(12), p. 121006.
[274] Stewart, W. C., 1968, "Current Voltage Characteristics of Josephson Junctions," Appl. Phys. Lett., **12**(8), pp. 277–280.
[275] Keizer, J., and Smith, G. D., 1998, "Spark-to-Wave Transition: Saltatory Transmission of Calcium Waves in Cardiac Myocytes," Biophys. Chem., **72**(12), pp. 87–100.
[276] Scott, A. C., 1975, "The Electrophysics of a Nerve Fiber," Rev. Mod. Phys., **47**(2), pp. 487–533.

[277] Rotermund, H. H., Jakubith, S., von Oertzen, A., and Ertl, G., 1991, "Solitons in a Surface Reaction," Phys. Rev. Lett., **66**(23), pp. 3083–3086.
[278] Comte, J. C., Marquie, P., and Remoissenet, M., 1999, "Dissipative Lattice Model With Exact Traveling Discrete Kink-Soliton Solutions: Discrete Breather Generation and Reaction Diffusion Regime," Phys. Rev. E, **60**(6), pp. 7484–7489.
[279] Balk, A. M., Cherkaev, A. V., and Slepyan, L. I., 2001, "Dynamics of Chains With Non-Monotone Stress Strain Relations. II. Nonlinear Waves and Waves of Phase Transition," J. Mech. Phys. Solids, **49**(1), pp. 149–171.
[280] Truskinovsky, L., and Vainchtein, A., 2005, "Kinetics of Martensitic Phase Transitions: Lattice model," SIAM J. Appl. Math., **66**(2), pp. 533–553.
[281] Braun, O. M., Kivshar, Y. S., and Zelenskaya, I. I., 1990, "Kinks in the Frenkel-Kontorova Model With Long-Range Interparticle Interactions," Phys. Rev. B, **41**(10), pp. 7118–7138.
[282] Abeyaratne, R., and Knowles, J., 1991, "Kinetic Relations and the Propagation of Phase Boundaries in Solids," Arch. Ration. Mech. Anal., **114**(2), pp. 119–154.
[283] Remoissenet, M., and Peyrard, M., 1984, "Soliton Dynamics in New Models With Parametrized Periodic Double-Well and Asymmetric Substrate Potentials," Phys. Rev. B, **29**(6), pp. 3153–3166.
[284] Benichou, I., Faran, E., Shilo, D., and Givli, S., 2013, "Application of a Bi-Stable Chain Model for the Analysis of Jerky Twin Boundary Motion in Ni–Mn–Ga," Appl. Phys. Lett., **102**(1), p. 011912.
[285] Frazier, M. J., and Kochmann, D. M., 2017, "Band Gap Transmission in Periodic Bistable Mechanical Systems," J. Sound Vib., **388**, pp. 315–326.
[286] Chen, B. G., Upadhyaya, N., and Vitelli, V., 2014, "Nonlinear Conduction Via Solitons in a Topological Mechanical Insulator," Proc. Natl. Acad. Sci., **111**(36), pp. 13004–13009.
[287] Frazier, M. J., and Kochmann, D. M., 2017, "Atomimetic Mechanical Structures With Nonlinear Topological Domain Evolution Kinetics," Adv. Mater., **29**(19), p. 1605800.
[288] Zirbel, S. A., Tolman, K. A., Trease, B. P., and Howell, L. L., 2016, "Bistable Mechanisms for Space Applications," PLoS One, **11**, p. e0168218.
[289] Benichou, I., and Givli, S., 2015, "Rate Dependent Response of Nanoscale Structures Having a Multiwell Energy Landscape," Phys. Rev. Lett., **114**(9), p. 095504.
[290] Cherkaev, A., and Zhornitskaya, L., 2005, "Protective Structures With Waiting Links and Their Damage Evolution," Multibody Syst. Dyn., **13**(1), pp. 53–67.
[291] Evans, A., and Cannon, R., 1986, "Overview No. 48," Acta Metall., **34**(5), pp. 761–800.